# 13

# ITERATIVE TECHNIQUES FOR THE SOLUTION OF INTEGRAL EQUATIONS IN TRANSIENT ELECTROMAGNETIC SCATTERING

*A. G. Tijhuis*

## 13.1 Introduction

In this chapter, the transient scattering of electromagnetic waves by an obstacle of finite extent is investigated with the aid of the time-domain integral-equation technique. The numerical solution of transient scattering problems is possible using a variety of techniques, including finite-difference and finite-element methods. However, there are two distinct advantages in using integral equations. In the first place, the only spatial domain relevant in their solution is the interior or the boundary of the scattering object. Hence, we can restrict the computation to that domain. In the second place, radiation and causality conditions are inherently satisfied in any integral-equation formulation.

Historically, time-domain integral equations have first been solved with the aid of the *marching-on-in-time method.* In this method, one uses the common property of such equations, that the scattered field at each space-time point is expressed in terms of one or more integrals of field values at previous instants. Discretizing these integrals in space and time leads to a step-by-step updating procedure involving only a repeated linear combination of known field values.

The first application of the marching-on-in-time method pertained to transient scattering problems that can be formulated in terms of boundary integral equations. As far as acoustic scattering problems are concerned, the method was applied to two-and three-dimensional impenetrable obstacles with a variety of boundary conditions [1–8]. In electromagnetics, two- and three-dimensional perfectly conducting targets were analyzed during the same period as their acoustic counterparts [9–13]. For this class of problems, the development of the marching-on-in-time method has also been summarized in a number of review papers [14–17]. The second category of electromagnetic scattering problems that was solved is the transient scattering by homogeneous, lossless dielectric targets [18, 19].

When the scatterer is inhomogeneous, domain integral equations have to be resolved. For a number of three-dimensional acoustic and elastodynamic scattering problems, this was carried out in [20–22]. The two-dimensional acoustic case was dealt with in [23]. As far as electromagnetic scattering problems are concerned, to the best of the author's knowledge, only the dielectric slab [24–26] and the inhomogeneous, lossy dielectric cylinder [12, 13] have been investigated.

The most important difficulty in the application of the marching-

on-in-time method is the occurrence of exponentially increasing instabilities in the solutions obtained. These instabilities can be explained from the accumulation of the discretization errors in the time-recursive solution procedure. It is this problem that, in recent years, has diminished the interest in applying the method. One of the few exceptions is [27]. A number of researchers has attempted to control the error in the solutions obtained by either modifying the discretization or the formulation of the problem [12, 26, 28–30]. The success of such attempts has been limited, and appears to depend strongly on the structure of the integral equation at hand.

A more fundamental approach is to use a different method of solution. To this end, the numerical solution is redefined as the set of approximate field values that minimizes a squared error in the equality sign of the discretized integral equation. This solution is then obtained by applying a *gradient method* [21, 31], a *conjugate-gradient method* [32–36] or a *relaxation method* [37, Chapter 3].

The essential difference between a conjugate-gradient method and the relaxation method is that, in each iteration step, the former *totally* improves the component of the iterate along a *single* direction in the relevant solution space, while the latter *partially* improves the values along *all* wel-behaved eigenvectors of the system matrix of the discretized integral equation. This makes the relaxation method more suitable for determining a large solution vector corresponding to a fine space-time sampling of the unknown electromagnetic field.

In the present chapter, we give a tutorial review the state of affairs as it stands now. In Section 13.2, we present one way of deriving the relevant integral equations in a systematic manner. We end up with a general operator form that is representative of the entire class of equations, and that contains sufficient information to allow a discussion of the various computational procedures. In Section 13.3, we formulate and analyze the marching-on-in-time method. In particular, we propose a matrix interpretation of the discretized integral equation that explains the stability behavior of all time-marching results known to the author. The same interpretation is also used in Sections 13.4 and 13.5, where the conjugate-gradient method and the relaxation method are discussed. Finally, the conclusions are stated in Section 13.6. Throughout the chapter, the discussion is illustrated with the aid of representative numerical results. To preserve the tutorial character of the discussion, the examples were chosen as simple as possible.

Like any tutorial discussion, this chapter contains some material that has previously been published elsewhere. In particular, much of the information contained in Section 13.3 and 13.5 can also be found in [37]. Compared with that reference, the text has been completely rewritten. Additional results by this and other authors have been included, while, at a few places, it has been possible to come up with a better established or a more explicit analysis. Most of the material presented in Section 13.2 and 13.4 is new or has, until now, remained unpublished.

Much effort has been spent to arrive at a coherent account, from which a reader interested in time-domain integral equations can select the most appropriate approach for his or her problem. In this context, all programs have been (re)written in Fortran 77, and all computations were carried out on the same computer, a VAXstation 2000 running under version V5.0-2 of the VAX/VMS operating system.

## 13.2 Basic Equations

Although time-domain integral equations have been the subject of investigation for at least two decades, relatively little attention has been devoted in the open literature to their formulation. The most complete accounts were given by Poggio an Miller [14], and by Mittra [15]. In this section, we present one way of systematically obtaining such integral equations. The original idea emanates from De Hoop, who proposed it for the formulation of integral equations for three-dimensional frequency-domain problems [38]. In what follows, we carry his derivation over to time-domain problems in one, two and three dimensions.

### *13.2.1 Source Representations for Electromagnetic Fields*

The basic tool in the formulation is a system of integral relations that, for points of observation in a given domain in space, leads to a source-type integral representation for the electromagnetic-field quantities.

We start with the situation where the electromagnetic-field quantities are defined in a bounded subdomain $\mathcal{D}_2$ of $\mathrm{R}^n$, with $n = 1, 2, 3$. The boundary of $\mathcal{D}_2$ is the closed surface $\partial\mathcal{D}$ (Fig. 13.2.1). $\partial\mathcal{D}$ is assumed to be sufficiently regular, i.e. the unit vector $\mathbf{n}$ along its outward

normal is a piecewise-continous vector of position. The unbounded domain exterior to $\partial\mathcal{D}$ is called $\mathcal{D}_1$. In $\mathcal{D}_2$, we assume an electric-current density $\mathcal{J}_D^e(\mathbf{r},t)$ and a magnetic-current density $\mathcal{J}_D^m(\mathbf{r},t)$ to be present in a homogeneous, lossless medium with constant permittivity $\epsilon$ and constant permeability $\mu$. The current densities appear as source terms in the electromagnetic-field equations, which are written as

$$\begin{aligned}\nabla\times\mathcal{H}(\mathbf{r},t)-\epsilon\partial_t\mathcal{E}(\mathbf{r},t)&=\mathcal{J}_D^e(\mathbf{r},t)\\ \nabla\times\mathcal{E}(\mathbf{r},t)+\mu\partial_t\mathcal{H}(\mathbf{r},t)&=-\mathcal{J}_D^m(\mathbf{r},t)\end{aligned}\tag{13.2.1}$$

The current densities $\mathcal{J}_D^e$ and $\mathcal{J}_D^m$ as well as the field quantities $\mathcal{E}$ and $\mathcal{H}$ are three-dimensional vectors, while the Cartesian position vector $\mathbf{r}$ and the corresponding gradient operator $\nabla$ are defined by

$$\mathbf{r}\stackrel{\text{def}}{=}\begin{cases}\mathbf{i}_x x & \text{for } n=1\\ \mathbf{i}_x x+\mathbf{i}_y y & \text{for } n=2\\ \mathbf{i}_x x+\mathbf{i}_y y+\mathbf{i}_z z & \text{for } n=3\end{cases}\tag{13.2.2}$$

and

$$\nabla\stackrel{\text{def}}{=}\begin{cases}\mathbf{i}_x\partial_x & \text{for } n=1\\ \mathbf{i}_x\partial_x+\mathbf{i}_y\partial_y & \text{for } n=2\\ \mathbf{i}_x\partial_x+\mathbf{i}_y\partial_y+\mathbf{i}_z\partial_z & \text{for } n=3\end{cases}\tag{13.2.3}$$

The time coordinate $t$ is chosen such that the current densities $\mathcal{J}_D^e(\mathbf{r},t)$ and $\mathcal{J}_D^m(\mathbf{r},t)$ as well as the field quantities $\mathcal{E}(\mathbf{r},t)$ and $\mathcal{H}(\mathbf{r},t)$ vanish for $t\le 0$.

Next, we transform the system of equations (13.2.1) into an equivalent system of algebraic equations. First, we introduce a temporal Laplace transform according to

$$\mathbf{E}(\mathbf{r},s)\stackrel{\text{def}}{=}\int_0^\infty dt\;\mathcal{E}(\mathbf{r},t)\exp(-st)\tag{13.2.4}$$

which is regular for $\mathrm{Re}(s)\ge 0$. This transformation reduces (13.2.1) to

$$\begin{aligned}\nabla\times\mathbf{H}(\mathbf{r},s)-s\epsilon\mathbf{E}(\mathbf{r},s)&=\mathbf{J}_D^e(\mathbf{r},s)\\ \nabla\times\mathbf{E}(\mathbf{r},s)+s\mu\mathbf{H}(\mathbf{r},s)&=-\mathbf{J}_D^m(\mathbf{r},s)\end{aligned}\tag{13.2.5}$$

Second, we define the spatial Fourier transform $\hat{\mathbf{V}}(\mathbf{k})$ of a vector field $\mathbf{V}(\mathbf{r})$ as

$$\hat{\mathbf{V}}(\mathbf{k})\stackrel{\text{def}}{=}\int_{\mathcal{D}_2} dV(\mathbf{r})\exp(-i\mathbf{k}\cdot\mathbf{r})\,\mathbf{V}(\mathbf{r})\tag{13.2.6}$$

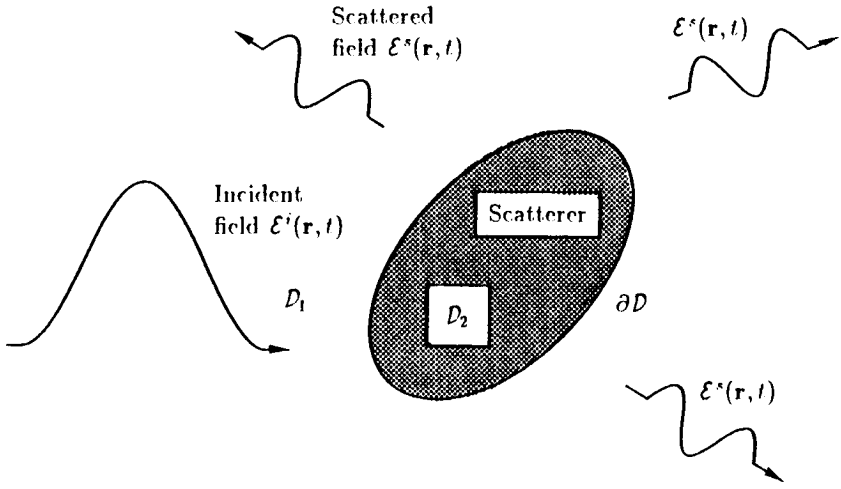


**Figure 13.2.1 Scattering of a pulsed electromagnetic wave by an obstacle of finite extent.**

where

$$\mathbf{k} = \begin{cases} k_x \mathbf{i}_x & \text{for } n = 1 \\ k_x \mathbf{i}_x + k_y \mathbf{i}_y & \text{for } n = 2 \\ k_x \mathbf{i}_x + k_y \mathbf{i}_y + k_z \mathbf{i}_z & \text{for } n = 3 \end{cases} \tag{13.2.7}$$

In order to apply this transformation to (13.2.5), we further need the corresponding transform of $\nabla \times \mathbf{V}(\mathbf{r})$. With the aid of Gauss' theorem, we find

$$\widehat{(\nabla \times \mathbf{V})}(\mathbf{k}) = i\mathbf{k} \times \hat{\mathbf{V}}(\mathbf{k}) + \oint_{\partial \mathcal{D}} dA(\mathbf{r}) \exp(-i\mathbf{k} \cdot \mathbf{r}) [\mathbf{n}(\mathbf{r}) \times \mathbf{V}(\mathbf{r})] \tag{13.2.8}$$

The second term on the right-hand side of (13.2.8) is just the spatial Fourier transform of the vector function $\mathbf{n}(\mathbf{r}) \times \mathbf{V}(\mathbf{r})$ over its domain of definition $\partial \mathcal{D}$. Combining (13.2.5)–(13.2.8), we obtain the following equations for $\hat{\mathbf{H}}(\mathbf{k}, s)$ and $\hat{\mathbf{E}}(\mathbf{k}, s)$:

$$\begin{aligned} i\mathbf{k} \times \hat{\mathbf{H}}(\mathbf{k}, s) - s\epsilon \hat{\mathbf{E}}(\mathbf{k}, s) &= \hat{\mathbf{J}}_D^e(\mathbf{k}, s) + \hat{\mathbf{J}}_B^e(\mathbf{k}, s) \\ i\mathbf{k} \times \hat{\mathbf{E}}(\mathbf{k}, s) + s\mu \hat{\mathbf{H}}(\mathbf{k}, s) &= -\hat{\mathbf{J}}_D^m(\mathbf{k}, s) - \hat{\mathbf{J}}_B^m(\mathbf{k}, s) \end{aligned} \tag{13.2.9}$$

in which $\hat{\mathbf{J}}_B^e(\mathbf{k},s)$ and $\hat{\mathbf{J}}_B^m(\mathbf{k},s)$ are the spatial transforms over the boundary $\partial\mathcal{D}$ of the quantities

$$\mathbf{J}_B^e(\mathbf{r},s) \stackrel{\text{def}}{=} -\,\mathbf{n}(\mathbf{r}) \times \mathbf{H}(\mathbf{r},s) \;\text{ when } \mathbf{r} \in \partial\mathcal{D} \tag{13.2.10}$$

and

$$\mathbf{J}_B^m(\mathbf{r},s) \stackrel{\text{def}}{=} \mathbf{n}(\mathbf{r}) \times \mathbf{E}(\mathbf{r},s) \;\text{ when } \mathbf{r} \in \partial\mathcal{D} \tag{13.2.11}$$

respectively. Note that in the right-hand sides of (13.2.10) and (13.2.11) the limiting values of the quantities upon approaching $\partial\mathcal{D}$ via $\mathcal{D}_2$ are to be taken. The structure of (13.2.9) leads to the interpretation that $\mathbf{J}_B^e(\mathbf{r},s)$ and $\mathbf{J}_B^m(\mathbf{r},s)$ are the Laplace-transformed source densities of the electric and magnetic surface currents.

The system of equations (13.2.9) is now in the desired algebraic form. Solving these equations yields

$$\begin{aligned}\hat{\mathbf{E}} \;=\; & (k^2 + s^2\epsilon\mu)^{-1} \left\{ -s\mu \left( \hat{\mathbf{J}}_D^e + \hat{\mathbf{J}}_B^e \right) \right. \\ & \left. + (s\epsilon)^{-1}\, i\mathbf{k} \left[ i\mathbf{k} \cdot \left( \hat{\mathbf{J}}_D^e + \hat{\mathbf{J}}_B^e \right) \right] - i\mathbf{k} \times \left( \hat{\mathbf{J}}_D^m + \hat{\mathbf{J}}_B^m \right) \right\}\end{aligned} \tag{13.2.12}$$

and

$$\begin{aligned}\hat{\mathbf{H}} \;=\; & (k^2 + s^2\epsilon\mu)^{-1} \left\{ -s\epsilon \left( \hat{\mathbf{J}}_D^m + \hat{\mathbf{J}}_B^m \right) \right. \\ & \left. + (s\mu)^{-1}\, i\mathbf{k} \left[ i\mathbf{k} \cdot \left( \hat{\mathbf{J}}_D^m + \hat{\mathbf{J}}_B^m \right) \right] + i\mathbf{k} \times \left( \hat{\mathbf{J}}_D^e + \hat{\mathbf{J}}_B^e \right) \right\}\end{aligned} \tag{13.2.13}$$

where we have employed the usual notation $k \stackrel{\text{def}}{=} |\mathbf{k}| = (\mathbf{k} \cdot \mathbf{k})^{\frac{1}{2}}$.

In Subsection (13.2.2), it will be shown that the factor

$$\hat{G}(\mathbf{k},s) \stackrel{\text{def}}{=} \left(k^2 + s^2/c^2\right)^{-1} \tag{13.2.14}$$

with $c \stackrel{\text{def}}{=} (\epsilon\mu)^{-\frac{1}{2}}$ being the wave speed in the homogeneous medium, corresponds to a causal, $n$-dimensional space-time Green's function $\mathcal{G}(r,t)$, with $\mathcal{G}(r,t) = 0$ for $t < r/c$. This correspondence allows us to identify the right-hand sides of (13.2.12) and (13.2.13) in terms of space-time convolution integrals. In the case of the space integrals,

we have to account for the domain over which the relevant forward transformations are defined. We end up with

$$\left\{1, \frac{1}{2}, 0\right\} \mathcal{E}(\mathbf{r},t) = -\mu\partial_t \left[\mathbf{\Pi}_D^e(\mathbf{r},t) + \mathbf{\Pi}_B^e(\mathbf{r},t)\right] + \epsilon^{-1} \int_{-\infty}^{t} dt' \nabla \left\{\nabla \cdot \left[\mathbf{\Pi}_D^e(\mathbf{r},t') + \mathbf{\Pi}_B^e(\mathbf{r},t')\right]\right\} - \nabla \times \left[\mathbf{\Pi}_D^m(\mathbf{r},t) + \mathbf{\Pi}_B^m(\mathbf{r},t)\right] \tag{13.2.15}$$

and

$$\left\{1, \frac{1}{2}, 0\right\} \mathcal{H}(\mathbf{r},t) = -\epsilon\partial_t \left[\mathbf{\Pi}_D^m(\mathbf{r},t) + \mathbf{\Pi}_B^m(\mathbf{r},t)\right] + \mu^{-1} \int_{-\infty}^{t} dt' \nabla \left\{\nabla \cdot \left[\mathbf{\Pi}_D^m(\mathbf{r},t') + \mathbf{\Pi}_B^m(\mathbf{r},t')\right]\right\} + \nabla \times \left[\mathbf{\Pi}_D^e(\mathbf{r},t) + \mathbf{\Pi}_B^e(\mathbf{r},t)\right] \tag{13.2.16}$$

for $\mathbf{r} \in \{\mathcal{D}_2, \partial\mathcal{D}, \mathcal{D}_1\}$. In (13.2.15) and (13.2.16), we have introduced the potentials

$$\mathbf{\Pi}_D^{e,m}(\mathbf{r},t) \stackrel{\text{def}}{=} \int_{\mathcal{D}_2} dV(\mathbf{r}') \int_0^{t-R/c} dt'\, \mathcal{G}(R, t-t') \mathcal{J}_D^{e,m}(\mathbf{r}', t') \tag{13.2.17}$$

$$\mathbf{\Pi}_B^{e,m}(\mathbf{r},t) \stackrel{\text{def}}{=} \oint_{\partial\mathcal{D}} dA(\mathbf{r}') \int_0^{t-R/c} dt'\, \mathcal{G}(R, t-t') \mathcal{J}_B^{e,m}(\mathbf{r}', t') \tag{13.2.18}$$

with $R \stackrel{\text{def}}{=} |\mathbf{r} - \mathbf{r}'|$.

It should be pointed out that, in writing down (13.2.15) and (13.2.16), we have systematically translated the factors $i\mathbf{k}$ and $s$ occurring in (13.2.12) and (13.2.13) into space and time differentiations acting on the complete space-time integrals. For the time differentiations and integrations, an alternative translation is obtained by attributing the factors of $s$ in (13.2.12) and (13.2.13) to the corresponding operations acting on $\mathcal{J}_{D,B}^{e,m}(\mathbf{r}', t')$.

For the space differentiations, such an ambiguity is not available because of the finite extent of the domains of definition of the spatial Fourier transforms. Nevertheless, we still have some freedom. For

two-dimensional problems, for example, it may be convenient to incorporate the elaboration of one or more space differentations in the Fourier inversion procedure for the Green's function discussed in Subsection (13.2.2). Then, each space differentation produces a factor of $s$. These factors, too, can be attributed to time differentiations acting on either the complete space-time integrals or the current distribitions $\mathcal{J}^{e,m}_{D,B}(\mathbf{r}',t')$.

With (13.2.15) and (13.2.16), we now have at our disposal the basic integral relations for the integral-equation formulation of time-domain electromagnetic scattering problems in one, two or three dimensions.

### *13.2.2 Green's Functions*

The remaining issue from the analysis of Subsection 13.2.1 is the determination of the $n$-dimensional space-time domain Green's function $\mathcal{G}(\mathbf{r},t)$. Conventionally, $\mathcal{G}(\mathbf{r},t)$ is defined as the causal solution of the second-order differential equation

$$\left[\nabla^2 - \partial_t^2/c^2\right]\mathcal{G}(\mathbf{r},t) = -\delta(\mathbf{r})\delta(t) \tag{13.2.19}$$

where $c$ is the wave speed in some homogeneous background medium, and where $\nabla$ is the $n$-dimensional gradient operator specified in (13.2.3) Subjecting (13.2.19) to the temporal Laplace transformation (13.2.4) and to a spatial Fourier transformation over $\mathrm{R}^n$ results in

$$\hat{G}(\mathbf{k},s) = \left(k^2 + s^2/c^2\right)^{-1} \tag{13.2.20}$$

which is in agreement with the definition given in (13.2.14). Hence, $\mathcal{G}(\mathbf{r},t)$ can be obtained by carrying out the relevant inverse Laplace and Fourier inversion integrals for $n = 1,2,3$.

In all three cases, this is carried out in globally the same manner. First, $s$ is taken to be real and positive. This restriction facilitates the evaluation of one or more of the inversion integrals in

$$G(\mathbf{r},s) = \frac{1}{(2\pi)^n}\int_{\mathrm{R}^n} dV(\mathbf{k})\,\hat{G}(\mathbf{k},s)\,\exp(i\mathbf{k}\cdot\mathbf{r}) \tag{13.2.21}$$

with the aid of Cauchy's residue theorem and Jordan's lemma. Second, the result obtained is recognized as or reduced to a forward Laplace transform of the form (13.2.4). This allows us to invoke Lerch's theorem

[39], which states that a causal time signal $\mathcal{F}(t)$ is uniquely determined by its Laplace transform $F(s)$ for $s = s_0 + n\Delta s$, with $s_0$ and $\Delta s$ being real and positive, and with $n = 0, 1, 2, \ldots, \infty$. Third, the desired time-domain expression $\mathcal{G}(\mathbf{r}, t)$ is then obtained by inspection. In what follows, we will carry out this procedure for each case individually.

*Three Dimensions*

For $n = 3$, the easiest way is to introduce spherical coordinates in the $\mathbf{k}$-domain with the "vertical" axis in the direction of $\mathbf{r}$. The inversion integral (13.2.21) can then be written as

$$G(\mathbf{r}, s) = \frac{1}{8\pi^3} \int_0^\infty dk \int_0^\pi d\theta \int_{-\pi}^\pi d\phi \, \frac{k^2 \sin\theta}{k^2 + s^2/c^2} \exp(ikr\cos\theta) \tag{13.2.22}$$

Carrying out the integrations over the angular coordinates $\phi$ and $\theta$ results in

$$\begin{aligned} G(\mathbf{r}, s) &= \frac{1}{4\pi^2 ir} \int_0^\infty dk \, \frac{k}{k^2 + s^2/c^2} \left[\exp(ikr) - \exp(-ikr)\right] \\ &= \frac{1}{4\pi^2 ir} \int_{-\infty}^\infty dk \, \frac{k}{k^2 + s^2/c^2} \exp(ikr) \end{aligned} \tag{13.2.23}$$

In (13.2.23), the integral over $k$ is evaluated by decomposing the fraction of the integrand, closing the contour in the upper half of the complex $k$-plane, and applying Jordan's lemma and Cauchy's theorem. This leads to

$$G(\mathbf{r}, s) = G(r, s) = \exp(-sr/c)/4\pi r \tag{13.2.24}$$

Now, it is well known that the corresponding time signal is given by

$$\mathcal{G}(r, t) = \delta(t - r/c)/4\pi r \tag{13.2.25}$$

The difficulty, however, is to obtain $\mathcal{G}(r, t)$ *constructively*. Conventionally, this is achieved by realizing that (13.2.22)–(13.2.24) hold for any complex $s$ with $\mathrm{Re}(s) > 0$, and by evaluating the Bromwich inversion integral in

$$\int_{-\infty}^t \mathcal{G}(r, t')dt' = \frac{1}{2\pi i} \int_{\beta - i\infty}^{\beta + i\infty} \frac{1}{4\pi r s} \exp\left[s(t - r/c)\right] ds \tag{13.2.26}$$

with $\beta > 0$, by contour deformation in the complex $s$-plane. This results in

$$\int_{-\infty}^{t} \mathcal{G}(r,t')dt' = \mathcal{U}(t - r/c)/4\pi r \tag{13.2.27}$$

where $\mathcal{U}(t)$ denotes the unit time-step function. The differentiation of (13.2.27) with respect to $t$ in the sense of generalized functions then yields (13.2.25).

Compared with this derivation, Lerch's theorem provides a more natural inversion of (13.2.24). (13.2.24) is rewritten as

$$G(r,s) = \int_{0}^{\infty} dt\,[\delta(t - r/c)/4\pi r]\exp(-st) \tag{13.2.28}$$

from which $\mathcal{G}(r,t)$ is identified directly.

*Two Dimensions*

For $n = 2$, it is more convenient to describe $\mathbf{k}$-space by the original Cartesian coordinates. Again, we start by carrying out the spatial Fourier inversion

$$G(\boldsymbol{\rho},s) = \frac{1}{4\pi^2}\int_{-\infty}^{\infty} dk_y \int_{-\infty}^{\infty} dk_x \frac{\exp(ik_x x + ik_y y)}{k_x^2 + k_y^2 + s^2/c^2} \tag{13.2.29}$$

In (13.2.29), the $k_x$-integral is evaluated by decomposing the fraction in the integrand, closing the contour in the upper or lower half of the complex $k_x$-plane for $x < 0$ and $x > 0$, respectively, and applying Jordan's lemma and Cauchy's theorem. This yields

$$G(\boldsymbol{\rho},s) = \frac{1}{4\pi}\int_{-\infty}^{\infty} dk_y \frac{\exp\left(ik_y y - |x|\sqrt{k_y^2 + s^2/c^2}\right)}{\sqrt{k_y^2 + s^2/c^2}} \tag{13.2.30}$$

where $\mathrm{Re}\sqrt{k_y^2 + s^2/c^2} \geq 0$. The integral in (13.2.30) is now in a form amenable to the Cagniard-De Hoop method [40,41]. In this method, we utilize the fact that $s$ was taken real and positive to introduce the substitution $k_y = s\lambda/c$, with $\lambda$ being a real-valued, dimensionless parameter. We find

$$G(\boldsymbol{\rho},s) = \frac{1}{4\pi}\int_{-\infty}^{\infty} d\lambda \frac{\exp\left[s\left(i\lambda y - |x|\sqrt{\lambda^2 + 1}\right)/c\right]}{\sqrt{\lambda^2 + 1}} \tag{13.2.31}$$

Next, the contour is shifted in the complex $\lambda$-plane to the Cagniard-De Hoop contour. This contour is chosen such that the argument of the exponent in (13.2.31) is real-valued and nonnegative, i.e.

$$i\lambda y + |x|\sqrt{\lambda^2 + 1} = c\tau \tag{13.2.32}$$

with $\tau \geq 0$. Solving $\lambda$ from (13.2.32) results in

$$\lambda = \left(ic\tau y \pm |x|\sqrt{c^2\tau^2 - \rho^2}\right)/\rho^2, \ \rho/c < \tau < \infty \tag{13.2.33}$$

which, in turn, is a parameterization of one of the hyperbolas given by

$$\frac{\mathrm{Im}(\lambda)^2}{y^2} - \frac{\mathrm{Re}(\lambda)^2}{x^2} = \frac{1}{\rho^2} \tag{13.2.34}$$

As an illustration, the locations of the integration contours given in (13.2.31) and (13.2.33) and of the branch cuts of the square root in (13.2.31)–(13.2.32) in complex $\lambda$-plane are displayed in Fig. 13.2.2.

For $\lambda$ on the Cagniard-De Hoop contour, we have

$$\frac{d\lambda}{\sqrt{\lambda^2 + 1}} = \pm\frac{d\tau}{\sqrt{\tau^2 - \rho^2/c^2}} \tag{13.2.35}$$

where the $\pm$ signs correspond to the ones in (13.2.33). The contributions from the connecting segments at infinity vanish by Jordan's lemma. Taking into account the direction of the integration, we then arrive at

$$G(\boldsymbol{\rho}, s) = G(\rho, s) = \frac{1}{2\pi}\int_{\rho/c}^{\infty} d\tau \frac{\exp(-s\tau)}{\sqrt{\tau^2 - \rho^2/c^2}} \tag{13.2.36}$$

for $s$ real and positive. With Lerch's theorem, we finally obtain by inspection

$$\mathcal{G}(\rho, t) = \frac{\mathcal{U}(t - \rho/c)}{2\pi\sqrt{t^2 - \rho^2/c^2}} \tag{13.2.37}$$

in which $\mathcal{U}(t)$ is the unit time-step function.

As remarked in Subsection 13.2.1, the space-time functions corresponding to products of $\hat{G}(\mathbf{k}, s)$ and factors of $i\mathbf{k}$ can be obtained in

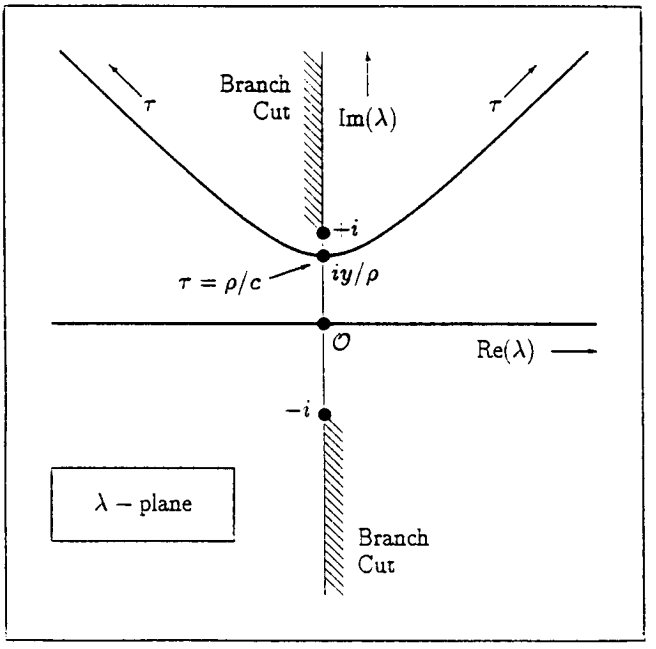


**Figure 13.2.2 Original integration contour as used in Equation (13.2.31) and Cagniard-De Hoop contour as specified in Equation (13.2.33), plotted in the complex $\lambda$-plane for $y > 0$.**

a similar way. For example, the integrals in the inverse Fourier transformation

$$\partial_y G(\boldsymbol{\rho}, s) = \frac{1}{4\pi^2} \int_{-\infty}^{\infty} dk_y \int_{-\infty}^{\infty} dk_x \, \frac{ik_y \exp(ik_x x + ik_y y)}{k_x^2 + k_y^2 + s^2/c^2} \tag{13.2.38}$$

reduce to

$$\partial_y G(\boldsymbol{\rho}, s) = \frac{is}{4\pi c} \int_{-\infty}^{\infty} d\lambda \, \frac{\lambda \exp\left[s\left(i\lambda y - |x|\sqrt{\lambda^2 + 1}\right)/c\right]}{\sqrt{\lambda^2 + 1}} \tag{13.2.39}$$

Shifting the path of integration to the Cagniard-De Hoop contour specified in (13.2.33), and substituting the intermediate results (13.2.33) and (13.2.35) yields

$$\partial_y G(\boldsymbol{\rho}, s) = \frac{-sy}{2\pi\rho^2} \int_{\rho/c}^{\infty} d\tau \, \frac{\tau \exp(-s\tau)}{\sqrt{\tau^2 - \rho^2/c^2}} \tag{13.2.40}$$

The factor of $s$ on the right-hand side can be translated into a time differentiation acting on the current distribution with which the Green's function is convolved. The remaining integral can again be converted to the time domain with the aid of Lerch's theorem. Moreover, the corresponding derivative with respect to $x$ is found immediately by interchanging $x$ and $y$ in the result. Hence, we have

$$\frac{i\mathbf{k}}{s}\hat{G}(\mathbf{k},s) \leftrightarrow -\mathbf{i}_\rho \frac{t\mathcal{U}(t-\rho/c)}{2\pi\rho\sqrt{t^2-\rho^2/c^2}} \tag{13.2.41}$$

where $\mathbf{i}_\rho \overset{\text{def}}{=} \boldsymbol{\rho}/\rho$. Similar expressions can also be obtained for products involving two or more factors of $i\mathbf{k}$.

*One Dimension*

For $n = 1$, we evaluate the Fourier inversion integral

$$G(x,s) = \frac{1}{2\pi}\int_{-\infty}^{\infty} dk_x \frac{\exp(ik_x x)}{k_x^2 + s^2/c^2} \tag{13.2.42}$$

by exactly the same procedure that was used for the $k_x$-integral in (13.2.29). Decomposing the fraction in the integrand, closing the contour in the upper or lower half of the complex $k_x$-plane for $x < 0$ and $x > 0$, respectively, and applying Jordan's lemma and Cauchy's theorem result in

$$G(x,s) = \frac{c}{2s}\exp(-s|x|/c) = \frac{c}{2}\int_{|x|/c}^{\infty} dt \exp(-st) \tag{13.2.43}$$

With the aid of Lerch's theorem, we therefore have

$$\mathcal{G}(x,t) = \frac{c}{2}\mathcal{U}(t-|x|/c) \tag{13.2.44}$$

where $\mathcal{U}(t)$ again denotes the unit time-step function.

*Discussion*

The procedure followed in this subsection may, at a first glance, seem somewhat artificial. As indicated above, the use of Lerch's theorem for $n = 3$ and $n = 1$ can be avoided by imposing a less severe restriction on $s$, so that $\mathcal{G}(\mathbf{r},t)$ is expressed as a Bromwich inversion

integral that, in turn, is amenable to contour deformation in the complex $s$-plane. However, the present derivation has the advantage of offering one and the same approach for both $n = 1, 2, 3$. In addition, the ambiguity problems inherent in second-order space-time differential equations of the type (13.2.19) are resolved automatically, by aiming for a causal solution right from the start. Finally, the procedure is capable of being generalized to configurations where the background medium is layered instead of homogeneous (for a description of the relevant techniques, see e.g. [42,43]).

### *13.2.3 Integral Equations for Scattering by Electrically Impenetrable Objects*

The theory developed in Subsections 13.2.1 and 13.2.2 will now be employed to derive integral equations suitable for the description of the transient scattering of pulsed electromagnetic waves by scattering objects embedded in a homogeneous, lossless medium. We restrict ourselves to the two cases that are most interesting from a practical point of view, i.e. those of electrically impenetrable (perfectly conducting) and inhomogeneous, lossy dielectric targets. In this subsection, we consider the impenetrable case.

Let us first consider the *scattered* field in the *exterior* domain $\mathcal{D}_1$. The field intensities $\mathcal{E}^s(\mathbf{r}, t)$ and $\mathcal{H}^s(\mathbf{r}, t)$ satisfy the electromagnetic-field equations

$$\begin{aligned} \nabla \times \mathcal{H}^s(\mathbf{r}, t) - \epsilon_1 \partial_t \mathcal{E}^s(\mathbf{r}, t) &= \mathbf{0}, \\ \nabla \times \mathcal{E}^s(\mathbf{r}, t) + \mu_1 \partial_t \mathcal{H}^s(\mathbf{r}, t) &= \mathbf{0} \end{aligned} \tag{13.2.45}$$

when $\mathbf{r} \in \mathcal{D}_1$. On account of this equation, (13.2.16) leads to

$$\begin{aligned} \left\{-1, -\frac{1}{2}, 0\right\} \mathcal{H}^s(\mathbf{r}, t) = \nabla \times \mathbf{\Pi}_B^{e,s}(\mathbf{r}, t) - \epsilon_1 \partial_t \mathbf{\Pi}_B^{m,s}(\mathbf{r}, t) \\ + \mu_1^{-1} \int_{-\infty}^{t} dt' \nabla [\nabla \cdot \mathbf{\Pi}_B^{m,s}(\mathbf{r}, t')] \end{aligned} \tag{13.2.46}$$

for $\mathbf{r} \in \{\mathcal{D}_1, \partial\mathcal{D}, \mathcal{D}_2\}$. In (13.2.46), the potentials $\mathbf{\Pi}$ are the ones defined in (13.2.18), while the additional superscript $s$ reflects the fact that these potentials now pertain to the scattered field. Obviously, the wave speed $c$ should be taken equal to $c_1 \stackrel{\text{def}}{=} (\epsilon_1 \mu_1)^{-\frac{1}{2}}$. Finally, the minus sign in (13.2.46) originates from the fact that $\mathbf{n}(\mathbf{r})$ points into $\mathcal{D}_1$.

In writing down (13.2.46), we have applied the integral relation (13.2.16) to an infinite domain. Strictly speaking, this is not allowed, since this relation was derived for a finite domain only. However, we can also arrive at (13.2.46) by considering the domain between $\partial\mathcal{D}$ and a second boundary at $r = r_\infty$. Using the property that the scattered field vanishes when $t \leq 0$, we can then make the contribution from this extra boundary vanish by choosing a sufficently large radius $r_\infty$.

Second, we consider the *incident* field in the *interior* domain $\mathcal{D}_2$. Since, by definition, the incident field is the field that would be present in absence of the scatterer, we have

$$\begin{aligned} \nabla \times \mathcal{H}^i(\mathbf{r},t) - \epsilon_1 \partial_t \mathcal{E}^i(\mathbf{r},t) &= 0 \\ \nabla \times \mathcal{E}^i(\mathbf{r},t) + \mu_1 \partial_t \mathcal{H}^i(\mathbf{r},t) &= 0 \end{aligned} \tag{13.2.47}$$

when $\mathbf{r} \in \mathcal{D}_2$. In (13.2.47), the right-hand sides contain no source terms since the sources of the incident field are located in $\mathcal{D}_1$. Equation (13.2.16) then leads to

$$\begin{aligned} \left\{0, \frac{1}{2}, 1\right\} \mathcal{H}^i(\mathbf{r},t) = \nabla \times \mathbf{\Pi}_B^{e,i}(\mathbf{r},t) - \epsilon_1 \partial_t \mathbf{\Pi}_B^{m,i}(\mathbf{r},t) \\ + \mu_1^{-1} \int_{-\infty}^{t} dt' \nabla[\nabla \cdot \mathbf{\Pi}_B^{m,i}(\mathbf{r},t')] \end{aligned} \tag{13.2.48}$$

for $\mathbf{r} \in \{\mathcal{D}_1, \partial\mathcal{D}, \mathcal{D}_2\}$. In (13.2.48), the potentials refer to the incident field.

Third, we make use of the fact that the scatterer is electrically impenetrable. This provides us with the boundary condition

$$\mathcal{J}_B^{m,i}(\mathbf{r},t) + \mathcal{J}_B^{m,s}(\mathbf{r},t) = \mathcal{J}_B^{m}(\mathbf{r},t) = \mathbf{n}(\mathbf{r}) \times \mathcal{E}(\mathbf{r},t) = 0 \tag{13.2.49}$$

when $\mathbf{r} \in \partial\mathcal{D}$. This condition shows that we can obtain an integral equation involving only the magnetic-field strength $\mathcal{H}(\mathbf{r},t)$ by adding up (13.2.46) and (13.2.48). We end up with

$$\left\{1, \frac{1}{2}, 0\right\} \mathcal{H}(\mathbf{r},t) = \mathcal{H}^i(\mathbf{r},t) - \nabla \times \mathbf{\Pi}_B^{e}(\mathbf{r},t) \tag{13.2.50}$$

for $\mathbf{r} \in \{\mathcal{D}_1, \partial\mathcal{D}, \mathcal{D}_2\}$. For $\mathbf{r} \in \partial\mathcal{D}$ and $0 \leq t < \infty$, the relation (13.2.50) constitutes an integral equation of the second kind for the tangential components of the unknown magnetic field $\mathcal{H}(\mathbf{r},t)$.

Once this field is known, the normal components on $\partial\mathcal{D}$ and the field in $\mathcal{D}_1$ are obtained directly by evaluating the term $\nabla \times \mathbf{\Pi}_B^e(\mathbf{r},t)$ in (13.2.50). In principle, the formulation of the problem has therefore been completed.

In the literature [14], (13.2.50) is known as the magnetic-field integral equation (MFIE). Since it pertains to field values on $\partial\mathcal{D}$, it is of the *boundary* type. A similar integral equation can be obtained by considering the electric-field strength $\mathcal{E}(\mathbf{r},t)$ for $\mathbf{r} \in \partial\mathcal{D}$. However, this so-called electric-field integral equation (EFIE) is of the first kind, which makes it less suitable for a numerical solution. Therefore, we leave it out of consideration.

Finally, we are faced with the task of breaking down (13.2.50) to a form that is more appropriate for the application of the various numerical procedures. In particular, we still have to select the tangential field components on $\partial\mathcal{D}$, and we must evaluate the curl operation. In doing so, we distinguish between three- and two-dimensional scattering problems.

*Three Dimensions*

For $n = 3$, it is most common to take the cross-product with $\mathbf{n}(\mathbf{r})$, and to solve the integral equation for source density of electric surface current

$$\mathcal{J}_B^e(\mathbf{r},t) \stackrel{\text{def}}{=} -\mathbf{n}(\mathbf{r}) \times \mathcal{H}(\mathbf{r},t)$$

introduced in (13.2.10). With this definition and with (13.2.25), (13.2.50) can be rewritten as

$$\mathcal{J}_B^e(\mathbf{r},t) = 2\,\mathcal{J}_B^{e,i}(\mathbf{r},t) - \frac{1}{2\pi}\,\mathbf{n}(\mathbf{r}) \times \nabla \times \oint_{\partial\mathcal{D}} dA(\mathbf{r}')\,\frac{\mathcal{J}_B^e(\mathbf{r}',t - R/c_1)}{R} \tag{13.2.51}$$

for $\mathbf{r} \in \partial\mathcal{D}$. In (13.2.51),

$$\mathcal{J}_B^{e,i}(\mathbf{r},t) \stackrel{\text{def}}{=} -\mathbf{n}(\mathbf{r}) \times \mathcal{H}^i(\mathbf{r},t)$$

denotes the source density of electric surface current that corresponds to the incident field. Carrying out the curl operation results in

$$\mathcal{J}_B^e(\mathbf{r},t) = 2\mathcal{J}_B^{e,i}(\mathbf{r},t) - \frac{1}{2\pi}\oint_{\partial\mathcal{D}} dA(\mathbf{r}')\,\mathbf{n}(\mathbf{r}) \times \left[\left(\frac{1}{R^2} + \frac{1}{c_1 R}\partial_{t'}\right)\mathcal{J}_B^e(\mathbf{r}',t') \times \mathbf{i}_R\right] \tag{13.2.52}$$

where $t' \stackrel{\text{def}}{=} t - R/c_1$ and $\mathbf{i}_R \stackrel{\text{def}}{=} (\mathbf{r} - \mathbf{r}')/R$. When $\mathbf{n}(\mathbf{r})$ is piecewise differentiable with respect to the transverse coordinates on $\partial\mathcal{D}$, it is not necessary to consider the integral involved in (13.2.52) in the principal-value sense. From the definition (13.2.10), we have

$$\mathbf{n}(\mathbf{r}) \times \left[\mathcal{J}_B^e(\mathbf{r}', t') \times \mathbf{i}_R\right] = \left(\mathbf{i}_R \cdot \mathcal{H}(\mathbf{r}', t')\right)\left[\mathbf{n}(\mathbf{r}) \times \mathbf{n}(\mathbf{r}')\right] - \left(\mathbf{i}_R \cdot \mathbf{n}(\mathbf{r}')\right)\left[\mathbf{n}(\mathbf{r}) \times \mathcal{H}(\mathbf{r}', t')\right] \tag{13.2.53}$$

In the right-hand side, both $[\mathbf{n}(\mathbf{r}) \times \mathbf{n}(\mathbf{r}')]$ and $(\mathbf{i}_R \cdot \mathbf{n}(\mathbf{r}'))$ are of $\mathcal{O}(R)$ as $R \to 0$, while the remaining factors are $\mathcal{O}(1)$. Consequently, we have

$$\mathbf{n}(\mathbf{r}) \times \left[\mathcal{J}_B^e(\mathbf{r}', t') \times \mathbf{i}_R\right] = \mathcal{O}(R) \tag{13.2.54}$$

The numerical aspects of the integral equation (13.2.52) have been investigated by several authors [9, 17, 30, 44, 45]. A brief review of the results will be given in Subsection 13.3.5.

*Two Dimensions*

For $n = 2$, it is most convenient to evaluate the curl operation by using the equivalence between the integral relations (13.2.13) and (13.2.16). With the aid of the correspondence (13.2.41), we immediately find

$$-\nabla \times \mathbf{\Pi}_B^e(\rho, t) = \frac{1}{2\pi} \oint_{\partial\mathcal{D}} dS(\boldsymbol{\rho}') \frac{\mathbf{i}_R}{R} \times \int_0^{t - R/c_1} dt' \frac{t - t'}{\sqrt{(t - t')^2 - R^2/c_1^2}} \partial_{t'} \mathcal{J}_B^e(\boldsymbol{\rho}', t') \tag{13.2.55}$$

with $\mathbf{i}_R \stackrel{\text{def}}{=} (\boldsymbol{\rho} - \boldsymbol{\rho}')/R$. Substitution of (13.2.55) and use of the definition of $\mathcal{J}_B^e(\boldsymbol{\rho}, t)$ in (13.2.50) then results in two scalar equations for the tangential field components of $\mathcal{H}(\boldsymbol{\rho}, t)$:

$$\begin{aligned} \mathcal{H}_z(\rho, t) &= 2\mathcal{H}_z^i(\rho, t) + \frac{1}{\pi} \oint_{\partial\mathcal{D}} dS(\boldsymbol{\rho}') \frac{(\mathbf{i}_R \cdot \mathbf{n}(\boldsymbol{\rho}'))}{R} \mathcal{I}_z(\boldsymbol{\rho}'; t, R) \\ \mathcal{H}_\tau(\rho, t) &= 2\mathcal{H}_\tau^i(\rho, t) + \frac{1}{\pi} \oint_{\partial\mathcal{D}} dS(\boldsymbol{\rho}') \frac{(\mathbf{i}_R \cdot \mathbf{n}(\boldsymbol{\rho}))}{R} \mathcal{I}_\tau(\boldsymbol{\rho}'; t, R) \end{aligned} \tag{13.2.56}$$

with

$$\mathcal{I}_{z,\tau}(\boldsymbol{\rho}';t,R)\stackrel{\text{def}}{=}\int_0^{t-R/c_1} dt' \frac{t-t'}{\sqrt{(t-t')^2-R^2/c_1^2}}\,\partial_{t'}\mathcal{H}_{z,\tau}(\boldsymbol{\rho}',t') \tag{13.2.57}$$

which hold when $\boldsymbol{\rho} \in \partial\mathcal{D}$. In (13.2.56) and (13.2.57), $\mathcal{H}_\tau(\boldsymbol{\rho},t)$ denotes the component along the tangential unit vector $\boldsymbol{\tau}(\boldsymbol{\rho})$. $\boldsymbol{\tau}(\boldsymbol{\rho})$ is chosen such that the three unit vectors $\{\mathbf{n}(\boldsymbol{\rho}),\boldsymbol{\tau}(\boldsymbol{\rho}),\mathbf{i}_z\}$ form a right-handed system.

A straightforward geometrical argument shows that, as $R \to 0$, the integrands of the $\boldsymbol{\rho}'$-integrals involved in (13.2.56) approach the values $-\mathcal{H}_z(\boldsymbol{\rho},t)/2a(\boldsymbol{\rho})$ and $\mathcal{H}_\tau(\boldsymbol{\rho},t)/2a(\boldsymbol{\rho})$, respectively, with $a(\boldsymbol{\rho})$ being the local radius of curvature. Therefore, as in the three-dimensional case, we need not take a principal value.

The special form of the integral equations (13.2.56) was first proposed in [12]. Previously, a different form had been used to resolve the present problem [9–10], and similar acoustic scattering problems [1–4]. This "original" form is obtained by substituting (13.2.37) in (13.2.50), and by carrying out the curl operation directly. The main advantages of (13.2.56) lie in the numerical implementation. Details can be found in [37, Subsection 3.4.1].

### *13.2.4 Integral Equations for Scattering by Inhomogeneous, Lossy Dielectric Objects*

To illustrate how the theory developed in Subsections 13.2.1 and 13.2.2 can be employed to derive *domain* integral equations, we now turn our attention to the transient scattering of pulsed electromagnetic waves by inhomogeneous, lossy dielectric objects.

In particular, we consider the case where, in $\mathcal{D}_1$, we have a homogeneous, lossless dielectric with permeability $\mu(\mathbf{r}) = \mu_0$, permittivity $\epsilon(\mathbf{r}) = \epsilon_1$, and conductivity $\sigma(\mathbf{r}) = 0$, and, in $\mathcal{D}_2$, an inhomogeneous, lossy dielectric with $\mu(\mathbf{r}) = \mu_0$, $\epsilon(\mathbf{r}) = \epsilon_2(\mathbf{r}) \geq \epsilon_0$, and $\sigma(\mathbf{r}) = \sigma_2(\mathbf{r}) \geq 0$. As usual, $\mu_0$ and $\epsilon_0$ denote the permeability and the permittivity of vacuum, respectively. The restriction to $\mu(\mathbf{r}) = \mu_0$ is not essential. The main motivation for this choice is that it leads to relatively simple expressions. Further, it applies to most practical dielectric materials.

For this configuration, Maxwell's equations reduce to

$$\nabla \times \mathcal{H}(\mathbf{r},t) - \epsilon(\mathbf{r})\partial_t\mathcal{E}(\mathbf{r},t) = \sigma(\mathbf{r})\mathcal{E}(\mathbf{r},t)$$

$$\nabla \times \mathcal{E}(\mathbf{r},t) + \mu_0 \partial_t \mathcal{H}(\mathbf{r},t) = \mathbf{0} \tag{13.2.58}$$

for all $\mathbf{r} \in \mathrm{R}^n$. For the incident field, i.e. the field that would be present in absence of the scatterer, we have

$$\begin{aligned} \nabla \times \mathbf{H}^i(\mathbf{r},t) - \epsilon_1 \partial_t \mathbf{E}^i(\mathbf{r},t) &= \mathbf{0} \\ \nabla \times \mathbf{E}^i(\mathbf{r},t) + \mu_0 \partial_t \mathbf{H}^i(\mathbf{r},t) &= \mathbf{0} \end{aligned} \tag{13.2.59}$$

for $\mathbf{r} \in \mathrm{R}^n$. The electromagnetic-field equations for the scattered field are obtained directly by substracting (13.2.59) from (13.2.58). This yields

$$\begin{aligned} \nabla \times \mathcal{H}^s(\mathbf{r},t) - \epsilon_1 \partial_t \mathcal{E}^s(\mathbf{r},t) &= \mathcal{J}_D^e(\mathbf{r},t), \\ \nabla \times \mathcal{E}^s(\mathbf{r},t) + \mu_0 \partial_t \mathcal{H}^s(\mathbf{r},t) &= \mathbf{0} \end{aligned} \tag{13.2.60}$$

with

$$\mathcal{J}_D^e(\mathbf{r},t) \stackrel{\text{def}}{=} \{[\epsilon(\mathbf{r}) - \epsilon_1]\,\partial_t + \sigma(\mathbf{r})\}\,\mathcal{E}(\mathbf{r},t) \tag{13.2.61}$$

being a contrast-source polarization current density. From the specification of the medium parameters given above it is observed immediately that $\mathcal{J}_D^e(\mathbf{r},t)$ is localized in $\mathcal{D}_2$.

Now, we can use the fact that the time coordinate $t$ is chosen such that the incident field does not reach the scatterer before $t = 0$. Therefore, causality ensures that the scattered field in $\mathcal{D}_1$ and $\mathcal{D}_2$ as well as the total field in $\mathcal{D}_2$ vanishes in the time interval $-\infty < t \leq 0$. By virtue of the same argument that we used in writing down (13.2.46), we can then apply the relation (13.2.15) to the scattered field in the entire space $\mathrm{R}^n$. This results in

$$\mathcal{E}(\mathbf{r},t) = \mathcal{E}^i(\mathbf{r},t) - \mu_0 \partial_t \mathbf{\Pi}_D^e(\mathbf{r},t) + \epsilon_1^{-1} \int_{-\infty}^{t} dt' \nabla \left[\nabla \cdot \mathbf{\Pi}_D^e(\mathbf{r},t')\right] \tag{13.2.62}$$

with $\mathbf{\Pi}_D^e(\mathbf{r},t)$ as defined in (13.2.17), in which the wave speed $c$ is taken equal to $c_1 \stackrel{\text{def}}{=} (\epsilon_1 \mu_0)^{-\frac{1}{2}}$.

For $\mathbf{r} \in \mathcal{D}_2$ and $0 \leq t < \infty$, the relation (13.2.62) constitutes an integral equation of the second kind for the unknown electric field $\mathcal{E}(\mathbf{r},t)$. Once this field is known, the field in $\mathcal{D}_1$ can be obtained directly by evaluating the terms involving $\mathbf{\Pi}_D^e(\mathbf{r},t)$ in the right-hand side of (13.2.62).

To the best of the author's knowledge, the full three-dimensional version of (13.2.62) has never been tackled numerically. Related problems from elastodynamics and acoustics have been investigated by Herman [20–22]. Electromagnetic applications have, until now, been reported only for the transient scattering of an electrically polarized, pulsed wave by an inhomogeneous, lossy dielectric slab, and by an inhomogeneous, lossy dielectric cylinder. In both these cases, (13.2.62) simplifies to a scalar integral equation of the form

$$\mathcal{E}_z(\mathbf{r},t) = \mathcal{E}_z^i(\mathbf{r},t) - \mu_0 \partial_t \Pi_{D,z}^e(\mathbf{r},t) \tag{13.2.63}$$

where $\Pi_{D,z}^e(\mathbf{r},t)$ denotes the $z$-component of the vector potential $\mathbf{\Pi}_D^e(\mathbf{r},t)$ figuring in (13.2.62). With (13.2.62) and (13.2.63), the formulation of the problem has been completed. What is left is the elaboration of the contrast term in (13.2.63). Since the explicit forms will be needed in subsequent discussions, we include them here for both $n = 1, 2$.

*Two Dimensions*

For $n = 2$, we substitute (13.2.37) and (13.2.17) in (13.2.63). Using the ambiguity with respect to placing time differentiations signalized towards the end of Subsection 13.2.1, we end up with

$$\mathcal{E}_z(\boldsymbol{\rho},t) = \mathcal{E}_z^i(\boldsymbol{\rho},t) - \frac{\mu_0}{2\pi} \int_{\mathcal{D}_2} dA(\boldsymbol{\rho}') \int_0^{t-R/c_1} dt' \frac{\partial_{t'} \mathcal{J}_{D,z}^e(\boldsymbol{\rho}',t')}{\sqrt{(t-t')^2 - R^2/c_1^2}} \tag{13.2.64}$$

where $\mathcal{J}_{D,z}^e(\boldsymbol{\rho}',t')$ denotes the $z$-component of the contrast-source polarization current density introduced in (13.2.61).

The integrand of the space integration in (13.2.64) has a logarithmic singularity as $R \to 0$. In fact, we have the estimate

$$\int_0^{t-R/c_1} dt' \frac{f(t')}{\sqrt{(t-t')^2 - R^2/c_1^2}} = -f(t) \ln(R/a) + \text{constant} + \mathcal{O}[R^2 \ln(R/a)] \tag{13.2.65}$$

where $a$ is a characteristic length, and where $f(t)$ denotes a sufficiently differentiable real-valued time signal. This estimate can be obtained by either transforming the left-hand side of (13.2.65) to the time-Laplace domain, or carrying out a repeated partial integration with respect to $t'$.

The numerical solution of the integral equation (13.2.64) and of a related form for a two-dimensional acoustic scattering problem has been investigated independently by a number of authors ([12, 13, 23] and [37, Section 3.5]). Representative results will be presented and discussed in Subsections 13.3.5 and 13.5.3.

*One Dimension*

For $n = 1$, the domain $\mathcal{D}_2$ is nothing but an interval of finite length $d$, which we will locate at $0 < x < d$. Substituting the one-dimensional space time Green's function given in (13.2.44) in (13.2.17) then results in

$$\begin{aligned}\mu_0 \partial_t \Pi^e_{D,z}(x,t) &= \frac{\mu_0 c_1}{2} \partial_t \int_0^d dx' \int_0^{t-|x-x'|/c_1} dt' \, \mathcal{J}^e_{B,z}(x',t') \\ &= \frac{Z_1}{2} \int_0^d dx' \, \mathcal{J}^e_{B,z}(x', t - |x-x'|/c_1) \qquad (13.2.66)\end{aligned}$$

with $Z_1 \stackrel{\text{def}}{=} (\mu_0/\epsilon_1)^{\frac{1}{2}}$. With the definition of the contrast-source polarization current density introduced in (13.2.61), we finally arrive at the well-known integral equation for transient scattering by a slab:

$$\mathcal{E}_z(x,t) = \mathcal{E}^i_z(x,t) - \frac{Z_1}{2} \int_0^d dx' \, [\Delta\epsilon(x')\partial_t + \sigma_2(x')] \, \mathcal{E}_z(x', t - |x-x'|/c_1) \qquad (13.2.67)$$

where $\Delta\epsilon(x') \stackrel{\text{def}}{=} \epsilon_2(x') - \epsilon_1$. This equation has received wide attention in the literature. We mention in particular [24–26, 37]. Numerical results will be reviewed in Subsections 13.3.5, 13.4.4 and 13.5.3.

*13.2.5 Operator Formulation*

Integral equations of the type derived in Subsections 13.2.3 and 13.2.4 have a number of common features that can be exploited to devise computational schemes for their solution. To conclude this section, we highlight these features by introducing a general operator form. This form is not only representative of transient electromagnetic scattering problems, but it also describes a wide range of elastodynamic and acoustic problems. It will be used throughout this chapter in the formulation of the various computational schemes.

Not all information about the detailed structure of the operator equation will be needed at all times. To keep the discussion tractable,

therefore, we specify the form of the operator equation to a varying degree of abstraction. We start off with the most abstract form, and we account for more of the physical properties of transient scattering problems as we go along.

The most striking aspects of the theory developed in the previous subsections are:

- The resulting integral equations pertain to *linear* problems. This restriction originates from the definition of the source densities of electric and/or magnetic current given in (13.2.10, 13.2.11, 13.2.61). In principle, the formulation for dielectric obstacles presented in Subsection 13.2.4 includes nonlinear problems. However, the numerical solution of such problems lies outside the scope of the present chapter.
- The desired solution is a causal, space-time electromagnetic-field quantity. It may vary from a single component of an electric or magnetic field strength (or of a related surface current) to a combination of the full three-dimensional field vectors.
- The unknown field is excited by a *forcing function* that corresponds to a pulsed wave, incident from a homogeneous, lossless domain surrounding the scatterer.

To some extent, all of these properties are already reflected in the general form

$$Lu = f \tag{13.2.68}$$

where $L$ is a *linear* operator acting on the *unknown* field quantity $u(\mathbf{r},t)$, and where $f(\mathbf{r},t)$ is a known *forcing* function.

The second important property is of a more mathematical nature. By comparing the integral equations (13.2.52, 13.2.56, 13.2.64, 13.2.67), we observe the following:

- All integral equations to be considered are of the *second kind.* As remarked in Subsection 13.2.3, alternative equations of the *first kind* are available for some configurations. These equations, however, are less desirable from a numerical point of view, and need not be considered in the present context.

To incorporate this property, we write the linear operator $L$ as

$$L \stackrel{\text{def}}{=} I - K \tag{13.2.69}$$

where $I$ is the identity operator, and where $K$ is an operator acting on the unknown field in the scattering domain only.

Third, we make explicit some of the properties of the source-type integrals that occur on the right-hand sides of (13.2.52, 13.2.56, 13.2.64, 13.2.67):

- The space integration runs over some finite domain $\mathcal{D}$, which may be either the interior of the scatterer $\mathcal{D}_2$ or its boundary $\partial\mathcal{D}$.
- The time integration runs from $t' = 0$, when the incident pulse first hits the object, to $t' = t - R/c$, with $t$ being the instant of observation, and $R$ being the distance from the point of observation $\mathbf{r}$ to some point $\mathbf{r}' \in \mathcal{D}$. The wave-speed parameter $c$ is typically chosen equal to the velocity of electromagnetic waves in $\mathcal{D}_1$.
- The operators acting on $u(\mathbf{r}', t')$ depend on the time difference $t - t'$ only. This reflects the feature that the scattering configuration does not vary in time.

With these properties, the operator $K$ introduced in (13.2.69) can be elaborated into

$$Ku(\mathbf{r}, t) \stackrel{\text{def}}{=} \int_{\mathcal{D}} d\mathbf{r}' \int_0^{t-R/c} dt'\, k(\mathbf{r}, \mathbf{r}'; t - t')\, u(\mathbf{r}', t') \qquad (13.2.70)$$

where $k(\mathbf{r}, \mathbf{r}'; t - t')$ denotes a linear, local, instantaneous operator acting on $u(\mathbf{r}', t')$. Typically, $k(\mathbf{r}, \mathbf{r}'; t - t')$ is singular as $R \to 0$, and involves one or more time differentations.

Finally, we must do justice to the special role of the time coordinate. From the expressions in (13.2.15–13.2.18), it is noticed directly that the operator $k(\mathbf{r}, \mathbf{r}'; t - t')$ is always of the form

$$k(\mathbf{r}, \mathbf{r}'; t - t')u(\mathbf{r}', t') \stackrel{\text{def}}{=} \sum_{p=0}^{P} C_p(\mathbf{r})\, g_p(R, t - t')\, (\partial_{t'})^p\, u(\mathbf{r}', t') \qquad (13.2.71)$$

In (13.2.71), $C_p(\mathbf{r})$ denotes a scalar or tensorial *contrast* or *curvature* parameter; $g_p(r, t)$ represents a scalar function derived from one of the Green's functions obtained in (13.2.25, 13.2.37, 13.2.44). From the explicit integral equations (13.2.52, 13.2.56, 13.2.64, 13.2.67), finally, it is observed that $g_p(r, t)$ may be singular as $r \to 0$.

With the equations given in this subsection, we now have available both an abstract and an explicit formulation of the integral equations

governing electromagnetic transient-scattering problems. Therefore, we pass on to their numerical solution.

## 13.3 The Marching-on-in-Time Method

The most straightforward way to solve time-domain integral equations of the type derived in Section 13.2 is to utilize the property that the scattered field at each space-time point is expressed in terms of one or more integrals over the scattering domain $\mathcal{D}$ of field values at previous instants. This is the basis of the so-called *marching-on-in-time method*, which, at first glance, provides an efficient direct procedure for solving time-domain integral equations. Having such a procedure available would obviate the application of any iterative technique, and, hence, the existence of this chapter. However, difficulties can usually be expected due to the discretization of the multiple integral of the induced source densities of electric and/or magnetic current. The accumulation of the errors caused in this manner may even give rise to instabilities in the numerical results obtained.

In this section, we formulate the method, and we review the mechanisms governing the error accumulation. By doing so, we hope to supply the reader with the insights needed to understand the iterative techniques that will be described in Sections 13.4 and 13.5.

### *13.3.1 Formulation of the Method*

To formulate the marching-on-in-time method, it suffices to consider the integral equations up to the level of abstraction of (13.2.70). Combining (13.2.68–13.2.70) leads to the general form

$$u(\mathbf{r},t) = f(\mathbf{r},t) + \int_{\mathcal{D}} d\mathbf{r}' \int_0^{t-R/c} dt'\, k(\mathbf{r},\mathbf{r}';t-t')\, u(\mathbf{r}',t') \qquad (13.3.1)$$

We subsequently discretize this integral equation in space and time. First, we introduce a uniform spatial grid $\{\mathbf{r}_\alpha\}$ with mesh size $h$, and approximate the space integral in (13.3.1) with the aid of a suitable combination of quadrature rules. This involves dealing with the singular behavior of the operator $k$ as $R \to 0$. Second, we take $t = n\Delta t$, where $n = 0,1,\ldots,\infty$, and where the time step $\Delta t$ is chosen such that

$$\Delta t \overset{\text{def}}{=} \min\{R_{\alpha\alpha'}\}/c \qquad (13.3.2)$$

This implies approximating all time differentiations and integrations in the integral equation (13.3.1). We then end up with algebraic equations of the type

$$\tilde{u}(\alpha,n)=\tilde{f}(\alpha,n)+\sum_{\alpha'}\sum_{n'=0}^{n}\tilde{k}(\alpha,\alpha';n-n')\tilde{u}(\alpha',n') \tag{13.3.3}$$

where $n=0,1,\ldots,\infty$, and where $\tilde{f}(\alpha,n)\overset{\text{def}}{=}f(\mathbf{x}_\alpha,n\Delta t)$. Owing to the choice of $\Delta t$, the discretization (13.3.3) can usually be organized such that $\tilde{k}(\alpha,\alpha';0)=0$ if $\alpha\neq\alpha'$. In that case, the integral equation (13.3.3) is already lower-triangular with respect to the time index $n$. In any case, it can be reduced to lower-triangular form by inverting the diagonally dominant weighting matrix

$$w(\alpha,\alpha')\overset{\text{def}}{=}\delta_{\alpha,\alpha'}-\tilde{k}(\alpha,\alpha';0) \tag{13.3.4}$$

(see also [37, Subsection 3.2.1]). This results in

$$\tilde{u}(\alpha,n)=\sum_{\alpha'}w^{-1}(\alpha,\alpha')\Bigg\{\tilde{f}(\alpha',n)+\sum_{\alpha''}\sum_{n'=0}^{n-1}\tilde{k}(\alpha',\alpha'';n-n')\tilde{u}(\alpha'',n')\Bigg\} \tag{13.3.5}$$

In this equation, the field values $\{\tilde{u}(\alpha,n)\}$ are, for each fixed instant $n$, expressed in terms of the known forcing function $f(\mathbf{r},t)$ at the instant $t=n\Delta t$ and the field values $\{\tilde{u}(\alpha,n')\mid n'<n\}$, i.e. the numerical solution at previous instants. Hence, (13.3.5) can be solved by a step-by-step updating procedure involving only the linear combination, at each space point, of known field values.

In terms of matrix calculus, the system of equations (13.3.3) can be envisaged as a matrix equation of infinite dimension for the unknown vector $\{\tilde{u}(\alpha,n)\}$. In that perspective, (13.3.5) can be understood as being the result of reducing (13.3.3) to lower-triangular form. Moreover, the inversion of the weighting matrix $w(\alpha,\alpha')$, which effectuates this triangularization, need only be carried out once, at the beginning of the time-stepping procedure.

As remarked above, difficulties can be expected due to the discretization of the multiple integral in (13.3.1). Because of the error

made in this discretization, $\tilde{u}(\alpha, n)$ is only approximately equal to the actual sampled field value $u(\mathbf{r}_\alpha, n\Delta t)$. Since, in (13.3.5), each field value is computed from field values $\tilde{u}(\alpha', n')$ at previous instants, the computational errors caused in this manner will accumulate. As a consequence, the solution obtained may even become unstable. In the upcoming two subsections, we will analyze this error accumulation.

### *13.3.2 Error Accumulation*

To gain insight into the process of error accumulation, we consider two types of deviations. In the first place, we define the *discretization error* $D(\alpha, n)$ as the error resulting from approximating the integral in (13.3.1) for $\mathbf{r} = \mathbf{r}_\alpha$ and $t = n\Delta t$ by the discrete sum in (13.3.3) for the *exact* field $u(\mathbf{r}, t)$, i.e.

$$D(\alpha, n) \stackrel{\text{def}}{=} \int_{\mathcal{D}} d\mathbf{r}' \int_0^{n\Delta t - |\mathbf{r}_\alpha - \mathbf{r}'|/c} dt'\, k(\mathbf{r}_\alpha, \mathbf{r}'; n\Delta t - t')\, u(\mathbf{r}', t') - \sum_{\alpha'} \sum_{n'=0}^{n} \tilde{k}(\alpha, \alpha'; n - n')\, u(\mathbf{r}_{\alpha'}, n'\Delta t) \tag{13.3.6}$$

This error is not known in full detail, since $u(\mathbf{r}, t)$ is unknown. Nevertheless, its magnitude can be estimated from the continuity and/or differentiability properties of $u(\mathbf{r}, t)$, which are known.

In the second place, we define the *marching-on-in-time error* $\Delta u(\alpha, n)$ as the deviation between the sampled actual field value and the corresponding marching-on-in-time result, i.e.

$$\Delta u(\alpha, n) \stackrel{\text{def}}{=} u(\mathbf{r}_\alpha, n\Delta t) - \tilde{u}(\alpha, n) \tag{13.3.7}$$

In addition to these errors, we define the so-called *error growth* as the difference between the marching-on-in-time errors at two consecutive instants at the same space point, i.e. as $\Delta u(\alpha, n) - \Delta u(\alpha, n-1)$. By taking a suitable linear combination of (13.3.1, 13.3.3, 13.3.6), we find that this error growth is governed by the equation

$$\Delta u(\alpha, n) - \Delta u(\alpha, n-1) = D(\alpha, n) - D(\alpha, n-1) + \sum_{\alpha'} \sum_{n'=0}^{n} \tilde{k}(\alpha, \alpha'; n - n')[\Delta u(\alpha', n') - \Delta u(\alpha', n'-1)] \tag{13.3.8}$$

which is of the same form as the original time-marching equation (13.3.3). In (13.3.8), the role of the incident field is played by the discretization-error difference $D(\alpha,n) - D(\alpha,n-1)$.

In general, the discretization error $D(\alpha,n)$ consists entirely of interpolation errors. Each of these errors is proportional to some power of the mesh size $h$ and to some higher-order space or time derivative at a space-time point that lies within a specified space or time interval of length $\mathcal{O}(h)$. For a smoothly varying $u(\mathbf{r},t)$ and a sufficiently small $h$, these errors will contain a systematic part corresponding to the average values of these derivatives, and a randomly varying part due to the arbitrariness of the exact location of the space-time points within the intervals. By considering the discretization-error difference, we have eliminated most of the systematic part. Hence we may regard $D(\alpha,n)-D(\alpha,n-1)$ as an almost randomly varying variable. Since the systematic part of $D(\alpha,n)$ may be absent, we estimate the magnitude of this difference as

$$D(\alpha,n) - D(\alpha,n-1) = \mathcal{O}[D(\alpha,n)] \tag{13.3.9}$$

In terms of the matrix interpretation given towards the end of Subsection 13.3.1, this observation implies that $D(\alpha,n) - D(\alpha,n-1)$ has components of equal order of magnitude along each of the basis vectors that span the space of possible marching-on-in-time solutions $\{u(\alpha,n)\}$. This provides us with the key to the error analysis for the discretized equation (13.3.3).

*Global Error Accumulation*

Since (13.3.3) is a, presumably accurate, discretization of the well-posed integral equation (13.3.1), almost all of the eigenvectors of its system matrix will be of $\mathcal{O}(1)$. Therefore, the components of the "known vector" $D(\alpha,n) - D(\alpha,n-1)$ along the corresponding eigenvectors will not be amplified in the solution vector $\Delta u(\alpha,n) - \Delta u(\alpha,n-1)$. In the subspace spanned by these "well-behaved" eigenvectors, we then have, by induction, the worst-case estimate:

$$\Delta u(\alpha,n) \leq \mathcal{O}\left[n \max\left\{D(\alpha,n') \mid 0 \leq n' \leq n\right\}\right] \tag{13.3.10}$$

Now we should realize that, for scattering by passive obstacles, we are ususally only interested in the field values in some finite time interval

$0 < t < T_{max}$. Moreover, the interpolation errors constituting $D(\alpha, n)$ will generally add up to an estimate of the type

$$D(\alpha, n) = \mathcal{O}(h^m) \tag{13.3.11}$$

with $m$ a positive integer. With these two observations in mind, we conclude directly that the error in the subspace spanned by the "well-behaved" eigenvectors is at most proportional to

$$(T_{max}/h)\, h^m = T_{max}\, h^{m-1} \tag{13.3.12}$$

Hence, it can be controlled by organizing the discretization such that $m > 1$, and by choosing $h$ sufficiently small. Since this "well-behaved" subspace covers almost the entire space of possible solutions, we will designate the behavior found in (13.3.12) as *global* error accumulation.

In all probability, the worst-case estimate (13.3.12) it too pessimistic. In practice, we will usually have some averaging, which would be more compatible with the "statistical" estimate

$$\Delta u(\alpha, n) \leq \mathcal{O}\left[n^{\frac{1}{2}} \max\left\{D(\alpha, n') \mid 0 \leq n' \leq n\right\}\right] \tag{13.3.13}$$

which, in turn, predicts that the error towards the end of the time interval $0 < t < T_{max}$ will be proportional to

$$(T_{max}/h)^{\frac{1}{2}}\, h^m = (T_{max})^{\frac{1}{2}}\, h^{m-\frac{1}{2}} \tag{13.3.14}$$

This indicates that even for $m = 1$, i.e. for $D(\alpha, n) = \mathcal{O}(h)$, refining the discretization may reduce the global error in time-marching results.

*Local Error Accumulation*

For certain scattering configurations, the system matrix of (13.3.3) and (13.3.8) may also have a few "problematic" eigenvectors with small eigenvalues. In the numerical solution of (13.3.3), the components of the "random" vector $D(\alpha, n) - D(\alpha, n-1)$ along these eigenvectors will be amplified, and the result obtained will be unstable. Since this effect will be localized within the small subspace spanned by these eigenvectors, an error of this type is called a *local* error. This qualification does not imply a local behavior of the error in the space-time domain. Rather, it refers to an error behavior of a special, unwanted character.

Greater comprehension of these local errors can only be obtained when the integral equation (13.3.1) is specified in more detail. This will be carried out in the next subsection.

### *13.3.3 Stability Analysis*

To understand the stability behavior of marching-on-in-time results, we need to recall the structure of the kernel $k(\mathbf{r},\mathbf{r}';t-t')$ summarized in (13.2.71). In general, this kernel involves one or two time differentiations acting directly on $u(\mathbf{r}',t')$. In the discretization, the resulting derivatives have to be approximated by suitable difference formulas. For example, aiming at a second-order accuracy ($m = 2$ in (13.3.11)), we can approximate $\partial_{t'} u(\mathbf{r}',t')$ by a three-term backward difference rule based on quadratic time interpolation:

$$\partial_{t'} u(\mathbf{r}',t') = \left[\frac{3}{2}\,u(\mathbf{r}',t') - 2\,u(\mathbf{r}',t'-\Delta t) + \frac{1}{2}\,u(\mathbf{r}',t'-2\Delta t)\right] \Big/ \Delta t \tag{13.3.15}$$

which holds up to $\mathcal{O}(\Delta t^2)$ [46]. Moreover, the scalar functions $g_p(r,t)$ are singular at $r = 0$ for most multi-dimensional scattering problems.

For convenience, let us restrict ourselves to the case where $u(\mathbf{r},t)$ is scalar, and where $k(\mathbf{r},\mathbf{r}';t-t')$ contains only first-order time derivatives, i.e. $P = 1$ in (13.2.71). These choices cover two of the specific integral equations derived in Section 13.2. In that case, we can come up with the following simplified model of the discretized integral equation in (13.3.3). Let $v[n]$ and $g[n]$, with $n \in \mathbb{Z}$, be real-valued time-sequences that vanish for $n \leq 0$ and that satisfy the difference equation

$$\begin{aligned} v[n] + w_0 C \left\{\frac{3}{2}\,v[n] - 2\,v[n-1] + \frac{1}{2}\,v[n-2]\right\} \\ + w_1 C \left\{\frac{3}{2}\,v[n-1] - 2\,v[n-2] + \frac{1}{2}\,v[n-3]\right\} = g[n] \end{aligned} \tag{13.3.16}$$

In (13.3.16), $w_0$ and $w_1$ are real-valued, positive weighting factors with $w_1 > w_0$, and $C$ is a positive configuration parameter that corresponds to the coefficient $C_1(\mathbf{r})$ in (13.2.71). As remarked in Subsection 13.2.5, this parameter represents either the local contrast (for

| Term in (13.3.16) | Corresponding terms in (13.3.3) |
|---|---|
| $v[n]$ | Field at the point of observation $\tilde{u}(\alpha, n)$. |
| Term with $w_0$ | "Self term" in discretized integral. |
| Term with $w_1$ | Contribution from "neighboring" space-time points. |
| $g[n]$ | Forcing function $\tilde{f}(\alpha, n)$ plus contribution from remaining space-time points. |

**Table 13.3.1 Interpretation of terms in difference equation for $g_1(r,t)$ being *singular* as $r \to 0$.**

| Term in (13.3.16) | Corresponding terms in (13.3.3) |
|---|---|
| $v[n]$ | Field at the point of observation $\tilde{u}(\alpha, n)$. |
| Term with $w_0$ | Systematic contribution from points with "even" time delay. |
| Term with $w_1$ | Systematic contribution from points with "odd" time delay. |
| $g[n]$ | Forcing function $\tilde{f}(\alpha, n)$ plus remaining contribution from "previous" space-time points. |

**Table 13.3.2 Interpretation of terms in difference equation for $g_1(r,t)$ being *bounded* as $r \to 0$.**

penetrable obstacles) or the local curvature (for impenetrable obstacles). The terms in (13.3.16) may be viewed in two complementary ways, according to the behavior of $g_1(r,t)$ as $r \to 0$.

The interpretation of Table 13.3.1 holds when $g_1(r,t)$ is singular. The "self term" is the part of the discretized integral containing the time-derivative at the space-time point of observation, i.e. at $\mathbf{r} = \mathbf{r}_\alpha$, $t = n\Delta t$. Owing to the choice of $\Delta t$ in (13.3.2), the "neighboring" space-time points are the point $\mathbf{r} = \mathbf{r}_\alpha$ and its nearest neighbors on the spatial grid $\{\mathbf{r}_\alpha\}$ at $t = (n-1)\Delta t$. Since there is always more than one neighbor, it seems fair to assume that the contribution from these neighbors is larger than the "self term" i.e. $w_1 > w_0$.

The interpretation of Table 13.3.2 holds in the absence of a singularity in $g_1(r,t)$, and applies only when $u(\mathbf{r},t)$ exhibits some "systematic" behavior. In that case, we may have "systematic" contributions of approximately the same magnitude from the points with an "even" and an "odd" time delay. Hence, we may still have $w_1 > w_0$. This type of behavior is best illustrated with the help of specific examples.

Therefore, further discussion is postponed until Subsection 13.3.5.

In both interpretations, it is assumed that the sequence $g[n]$ varies gradually with $n$, and that $g[n]$ remains bounded as $n \to \infty$.

The model proposed above may be an oversimplification in two respects. In the first place, it presupposes a fixed relation between the field values represented by the left-hand side of (13.3.16). In the second place, assuming $g[n]$ to be smoothly varying and bounded restricts the stability analysis to the interaction between a few selected space-time points. However, the only consequence of these simplifications is that certain types of instabilities may be excluded from the analysis. This implies that at least the instabilities predicted by our model can be regarded as being realistic. Furthermore, we can take example of the so-called Von Neumann stability analysis for time-domain partial differential equations [47]. That analysis, which has proven to produce even quantitatively correct results, involves a similar restriction to the local structure of the discretized equations.

To obtain an impression of the instabilities associated with the difference equation (13.3.16), we introduce the two-sided $z$-transform of the time sequence $v[n]$ as

$$V(z) \stackrel{\text{def}}{=} \sum_{n=-\infty}^{\infty} v[n]\, z^{-n} \tag{13.3.17}$$

Since $v[n]$ is a causal sequence, it is always possible to find a region of convergence $|z| > z_0$ where this transform exists. Taking the $z$-transform of (13.3.16) and defining $G(z)$ as the $z$-transform of the input sequence $g[n]$, we arrive at

$$\begin{aligned} V(z) &= z^3 G(z)/P(z), \text{ with} \\ P(z) &= z^3 + w_0 C \left(\frac{3}{2}z^3 - 2z^2 + \frac{1}{2}z\right) \\ &\quad + w_1 C \left(\frac{3}{2}z^2 - 2z + \frac{1}{2}\right) \end{aligned} \tag{13.3.18}$$

The unknown sequence $v[n]$ is causal as well. Hence, it can formally be obtained by evaluating the inversion integral

$$v[n] = \frac{1}{2\pi i} \oint_C dz\, V(z)\, z^{n-1} = \frac{1}{2\pi i} \oint_C dz\, \frac{G(z)}{P(z)}\, z^{n+2} \tag{13.3.19}$$

with $C$ being a circular contour of a sufficiently large radius in the complex $z$-plane. Evaluating the integral with the aid of Cauchy's theorem results in residual contributions corresponding to the poles of $G(z)$ and to the zeros of $P(z)$. Since $g[n]$ remains bounded as $n \to \infty$, it follows directly from the definition (13.3.17) that $G(z)$ is analytic for $|z| > 1$. Consequently, all its poles lie inside the unit circle $|z| = 1$.

In the present stability analysis, we are only interested in the poles outside the unit circle. Hence, we need only investigate the zeros of $P(z)$. Each of these zeros corresponds to a residual contribution of the form

$$v_m[n] = \frac{G(z_m)}{P'(z_m)} (z_m)^{n+2} \tag{13.3.20}$$

where $n \in \mathrm{Z}$, and where the prime denotes differentation with respect to the argument. This implies that the difference equation (13.3.16) has exponentially increasing solutions if and only if one of the zeros $\{z_m \mid m = 1,2,3\}$ of $P(z)$ has a magnitude larger than one.

For the cubic polynomial $P(z)$ introduced in (13.3.18), the conditions for having a zero with $|z_m| > 1$ can be obtained in closed form. Analyzing $P(z)$ and its derivatives shows that $P(z)$ always has a single zero on the negative real $z$-axis. This zero is located in the subinterval $-\infty < z < -1$ when $P(-1) > 0$, i.e. when $w_1 > w_0$ and

$$C > (4w_1 - 4w_0)^{-1} \tag{13.3.21}$$

Moreover, from the sign distribution of $P(z)$ on the positive real $z$-axis, it is observed that, for the two remaining zeros $\{z_2, z_3\}$, we have either of the following situations.

- For a sufficiently large $C$, both $z_2$ and $z_3$ are located on the real $z$-interval $\frac{1}{3} < z < 1$, where the term proportional to $C$ in $P(z)$ is negative.
- Otherwise, $z_2$ and $z_3$ form a complex-conjugate pair off the real $z$-axis.

In the former case, $z_2$ and $z_3$ are obviously located inside the unit circle. In the latter case, their magnitudes can be estimated with the aid of the identity

$$|z_2|^2 = |z_3|^2 = z_2 z_3 = -w_1 C / 2z_1 \left[1 + \frac{3}{2} w_0 C\right] \tag{13.3.22}$$

(see [48, formula 3.8.2]). By direct substitution, it follows that

$$P\left(-w_1 C/2\left[1+\frac{3}{2}w_0 C\right]\right) > 0 \tag{13.3.23}$$

Since $P(z)$ becomes negative as $z \to -\infty$, we then have

$$z_1 < -w_1 C/2\left[1+\frac{3}{2}w_0 C\right] \tag{13.3.24}$$

which, in combination with (13.3.22), implies that $|z_2| = |z_3| < 1$.

Combining the results derived above, we arrive at the following conclusions.

- Under the assumption that the kernel $k(\mathbf{r},\mathbf{r}';t-t')$ contains only a single time derivative, numerically solving (13.3.3) will resemble solving the simplified equation (13.3.16).
- Consequently, a stable result will only be produced for a finite range of the configuration parameter $C$. When $C$ lies inside that range, the discretization error $D(\alpha,n)$ defined in (13.3.6) only excites exponentially decaying terms. In that case, we have only global error accumulation in the marching-on-in-time method, in accordance with one of the estimates (13.3.10) or (13.3.13). Hence, we can control the error by refining the discretization.
- When $C$ lies outside the stability range, the numerically obtained solution will contain an exponentially exploding, unstable component that alternates with $n$ (see also (13.3.20)).

Finally, it should be pointed out that the instability result derived above can be generalized to the case where $k(\mathbf{r},\mathbf{r}';t-t')$ involves second-order time derivatives. Such derivatives can be modeled by including a four-point backward difference formula based on cubic time interpolation in (13.3.16). Repeating the analysis for the thus extended difference equation leads to a quartic characteristic polynomial similar to $P(z)$ with a similar zero $z_1$ on the negative real $z$-axis, and a zero $z_2$ on the interval $0 < z < \frac{1}{2}$. Whether the remaining two zeros $\{z_3, z_4\}$ are located inside the unit circle remains to be decided, however.

*Avoiding the Instabilities*

The conclusions formulated in the preceding paragraph raise the question how the instabilities can be avoided.

The first method that comes to mind is to modify the discretization of the integral in (13.3.3) such that the weighting factors $w_0$ and $w_1$ are reduced. If this can be achieved, it follows from the instability condition (13.3.21) that the allowed range for the configuration parameter $C$ will be enlarged. Obviously, the modification should be such that the global error behavior described in Subsection 13.3.2 is not affected significantly.

Within that restriction, we have two possibilities. When $w_0$ and $w_1$ are both of $o(1)$ as $h \to 0$, reducing the mesh size $h$ will eliminate the instability. Whether this approach takes effect depends on the structure of the integral equation at hand. In Subsection 13.3.5, we will discuss cases where reducing $h$ removes instabilities, as well as a case where it actually causes an instability.

Alternatively, $w_0$ and $w_1$ can be reduced by replacing the approximations to the first- and second-order time derivatives with difference formulas having a double time step (e.g. by taking $2\Delta t$ instead of $\Delta t$ in (13.3.15)). At the cost of a minor increase in the discretization error, this extends the stability range of the relevant parameters by a factor of two and four, respectively. Moreover, doubling the time step shifts the stability problem to the combination of the "self term" and the contributions from the "next-nearest neighbors", which may have a smaller weighting factor. One consequence of doubling the time step is that the instabilities observed no longer behave as given in (13.3.20). Instead, the interplay of two exponentially increasing time sequences that alternate with the double time step is observed. Examples of the effectivenes of doubling the time step will be given in Subsection 13.3.5 as well.

A disadvantage of modifying the discretization of the integral might be that it still leaves us with a finite range of applicability. For the doubling of the time step in the difference formulas, this limitation is obvious. Reducing the mesh size results in a sharp increase in computation time.

A second method to avoid instabilities in marching-on-in-time results may be of use when the interpretation of Table 13.3.2 applies. In that case, the integral equation (13.3.1) and/or the forcing function $f(\mathbf{r},t)$ can sometimes be changed such that the unwanted "systematic" behavior in the solution $u(\mathbf{r},t)$ is avoided. Like the "systematic" behavior itself, this possibility is best explained in the context of the specific examples. Here, we mention it for completeness.

### *13.3.4 Choice of the Reference Medium*

An important issue associated with the marching-on-in-time method that is often overlooked is the choice of the background medium in contrast-source integral equations of the type (13.2.62).

In (13.2.62), (13.2.64) and (13.2.67), this background medium was tacitly taken as a homogeneous, lossless medium with permittivity $\epsilon(x) = \epsilon_1$. We should realize, however, that this amounts to expanding the unknown solution $\mathcal{E}(\mathbf{r}, t)$ solely in terms of waves that propagate with velocity $c_1$. Doing so may violate the principle of causality: it is possible to have destructive interference of waves traveling with a velocity larger than the local wave speed $c_2(\mathbf{r}) \stackrel{\text{def}}{=} [\epsilon_2(\mathbf{r})\mu_0]^{-\frac{1}{2}}$, but we cannot produce a wave with velocity $c_2(\mathbf{r})$ by constructive interference of waves propagating with a speed smaller than $c_2(\mathbf{r})$.

This means that, for a successful application of the marching-on-in-time method, we must have $c_1 \geq c_2(\mathbf{r})$ for all $\mathbf{r} \in \mathcal{D}_2$. In that case, we have $\epsilon_2(\mathbf{r}) - \epsilon_1 \geq 0$, which is commonly referred to as a "positive" velocity contrast. For "negative" velocity contrasts, i.e. for $\epsilon_2(\mathbf{r}) - \epsilon_1 < 0$, numerical experimentation has produced unstable time-marching results that appear to increase faster than exponentially with increasing $n$.

The simplest example where this problem arises is the integral equation for scattering by a slab given in (13.2.67) with $\epsilon_2(x) =$ *constant* and $\sigma_2(x) = 0$ [37, Section 3.3]. The incident field is the pulsed plane wave

$$\mathcal{E}_z^i(x,t) = \mathcal{F}(t - x/c_1) \tag{13.3.25}$$

where $\mathcal{F}(t)$ vanishes outside a finite interval $0 < t < T$. For this configuration, direct substitution shows that, in the space-time region $0 < x < d$ and $t < x/c_1$, $\mathcal{E}_z(x,t) = 0$ solves (13.2.67). It is this solution that is "picked up" by the marching-on-in-time method, irrespective of the accuracy of the discretization. The actual arrival of the directly transmitted pulse occurs at $t = x/c_2$. When $c_2 > c_1$, this instant lies before $t = x/c_1$, and the marching-on-in-time method cannot be applicable.

One way to overcome this problem is to construct a contrast-source integral equation of the type (13.2.62) with respect to a composite background medium that is at least as "fast" as the actual medium for all $\mathbf{r} \in \mathrm{R}^n$. For the slab problem, this can be achieved by considering a three-layer medium with $\epsilon(x) = \epsilon_0$ when $0 < x < d$ [37,

Section 3.3]. For multi-dimensional scattering problems, such an approach seems less feasible because of the effort that would be required to compute the space-time Green's function of a suitable background medium.

Recently, the above observations have been confirmed independently by carrying out a stability analysis of the type performed in Subsection 13.3.3 for the complete discretized version of (13.2.67). Interested readers are referred to [49].

### *13.3.5 Examples*

In order to obtain insight into the applicability of the theory developed in Subsections 13.3.2 and 13.3.3, we now consider its consequences for each of the specific integral equations (13.2.52, 13.2.56, 13.2.64, 13.2.67). The motivation for selecting these particular equations has been that each of them has been solved by more than one author, and that, in combination, their solutions exhibit all possible types of stability behavior.

We will not present the space-time discretizations in detail. For the present discussion, it suffices to state that, for all results given in this chapter, the discretization error $D(\alpha, n) = \mathcal{O}(h^2)$ as $h \to 0$, i.e. $m = 2$ in (13.3.11). More information about the numerical aspects can be found in the references cited below and in Subsections 13.2.3 and 13.2.4.

#### *Dielectric Slab*

For the dielectric slab specified in connection with (13.2.67), instabilities as described by Table 13.3.1 are ruled out, since the integrand of the $x'$-integral remains bounded as $x' \to x$. In fact, the coefficients $\tilde{k}(\alpha, \alpha'; n - n')$ consist of a factor of $\mathcal{O}(h)$ from the space integration, and a factor of $\mathcal{O}(h^{-1})$ from the time differentiation in the term involving $\Delta\epsilon(x')$, and, consequently, are of $\mathcal{O}(1)$ as $h \to 0$.

As far as the systematic behavior of Table 13.3.2 is concerned, we should realize that $\mathcal{E}_z(x, t)$ represents a pulsed plane wave which, due to repeated reflection at the slab's interfaces, travels backwards and forwards across the slab. For such a field, the discretization-error difference $D(\alpha, n) - D(\alpha, n - 1)$ will tend to average out along the domain of integration. Therefore, it seems plausible that the errors $D(\alpha, n)$ will not cause an unwanted systematic behavior in the resulting marching-on-in-time error $\Delta u(\alpha, n)$.

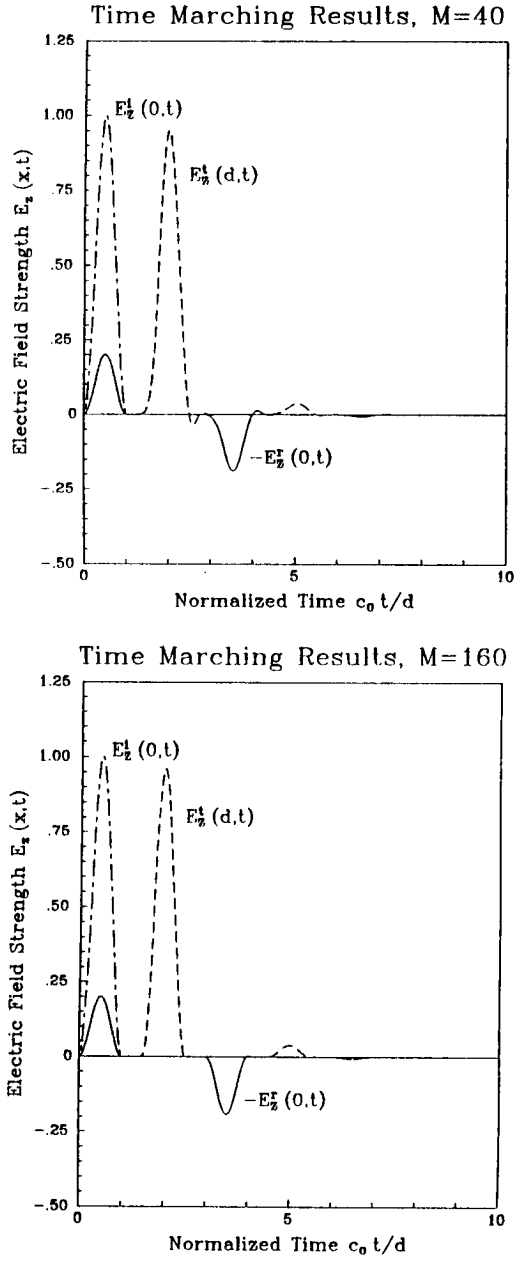


**Figure 13.3.1 Results of applying the marching-on-in-time method to the scattering of a sine-squared incident pulse of duration $c_0T/d = 1$ by a homogeneous, lossless slab with $\epsilon_{2r} = 2.25$ in free space: incident, reflected and transmitted fields at the slab's boundaries.**

| $M$ | *R.M.S. Error* | *C.P.U. Time* |
|---|---|---|
| 10 | 0.272 | 0.16s |
| 20 | 0.120 | 0.54s |
| 40 | 0.0385 | 2.01s |
| 80 | 0.0112 | 7.76s |
| 160 | 0.0032 | 29.34s |

**Table 13.3.3 Computational data of applying the marching-on-in-time method to the scattering of a sine-squared incident pulse of duration $c_0T/d = 1$ by a homogeneous, lossless dielectric slab with $\epsilon_{2r} = 2.25$ in free space.**

Representative results for the case of a homogeneous, lossless dielectric slab excited by a sine-squared incident pulse are given in Fig. 13.3.1 and Table 13.3.3. Figure 13.3.1. shows reflected and transmitted fields at the slab's boundaries, and Table 13.3.3 contains some computational data. $M$ is the number of subintervals in the numerical evaluation of the $x'$-integral, i.e. $h = d/M$. The root-mean-square error given in Table 13.3.3 is defined as $||\tilde{\mathcal{E}}_z - \mathcal{E}_z||/||\mathcal{E}_z||$, where $\mathcal{E}_z$ is the actual solution and $\tilde{\mathcal{E}}_z$ the marching-on-in-time result. The norm is defined as in (13.4.2).

From the results presented in Fig. 13.3.1 and Table 13.3.3, it is observed that the accuracy of the results indeed improves as $h \to 0$. From Fig. 13.3.1, we see that most of the error is contained in an overshoot at the "tail" of the successive pulses. This can be explained from the feature that, precisely at those space-time points, the approximation (13.3.15) is only accurate up to $\mathcal{O}(h)$.

In addition, Table 13.3.3 indicates that the error accumulation is of the "statistical" type resulting in (13.3.14). The computation time consumed is proportional to $M^2$, i.e. the number of unknown field values in the space-time domain under consideration. This efficiency originates from the feature in the numerical implementation that the $x'$-integrals on the right-hand side of (13.2.67) are evaluated recursively.

*Impenetrable Cylinder*

Scattering by an impenetrable (perfectly conducting) cylinder is described by the integral equations (13.2.56), in combination with the time integrals defined in (13.2.57). From (13.2.56) and (13.2.57), it is

observed that the integrand of the $\rho'$-integration is regular as $\rho' \to \rho$. This leaves us with the second interpretation of (13.3.16), in which a number of errors in the marching-on-in-time solution obtained add up systematically.

A special property of the integral equation (13.2.56) is that all the weighting factors $\tilde{k}(\alpha, \alpha'; n - n')$ in the discretized version are of $o(1)$ as $h \to 0$. This can be seen as follows. The time differentiation in (13.2.57) provides a factor of $\mathcal{O}(h^{-1})$, and the space integration in (13.2.56) a factor of $\mathcal{O}(h)$. Since the resulting product is of $\mathcal{O}(1)$, the factors $\tilde{k}(\alpha, \alpha'; n - n')$ will be of the same order of magnitude as the integral of the function

$$\frac{t - t'}{\sqrt{(t - t')^2 - R_{\alpha\alpha'}^2 / c_1^2}}$$

in (13.2.57) over an interval of length $\Delta t$. This leads to two different estimates. Near the end of the integration interval, we find

$$\tilde{k}(\alpha, \alpha'; n - n') = \mathcal{O}\left(h^{\frac{1}{2}}\right) \mathcal{O}\left(R_{\alpha\alpha'}^{\frac{1}{2}}\right)$$

because of the root-like singularity at $t' = t - R/c_1$. In the remainder of the integral, we have $\tilde{k}(\alpha, \alpha'; n - n') = \mathcal{O}(h)$. For space-time points near the point of observation, both estimates coincide, since for those points $R_{\alpha\alpha'} = \mathcal{O}(h)$. In view of these estimates, it seems plausible that, even for a systematic error, the parameters $w_0$ and $w_1$ in (13.3.16) decrease when the mesh size $h$ is reduced. As discussed towards the end of Subsection 13.3.3, this makes it possible to eliminate the instability by refining the discretization.

To illustrate how these considerations work out in a practical scattering problem, we have applied the marching-on-in-time method to the transient scattering by a perfectly conducting, circular cylinder of radius $a$. In Figure 13.3.2, results are presented for illumination by a magnetically polarized, sine-squared incident pulse. $M$ is the number of space points on the integration contour. Apparently, the field $\mathcal{H}_z(\rho, t)$ on the cylinder boundary exhibits no systematic behavior, and, consequently, an accurate, stable solution is obtained when the mesh size $h$ is fine enough.

Results for excitation by an electrically polarized incident pulse of the same duration are shown in Fig. 13.3.3. Now, the tangential magnetic field $\mathcal{H}_\tau(\rho, t)$ does show a systematic behavior since, for large

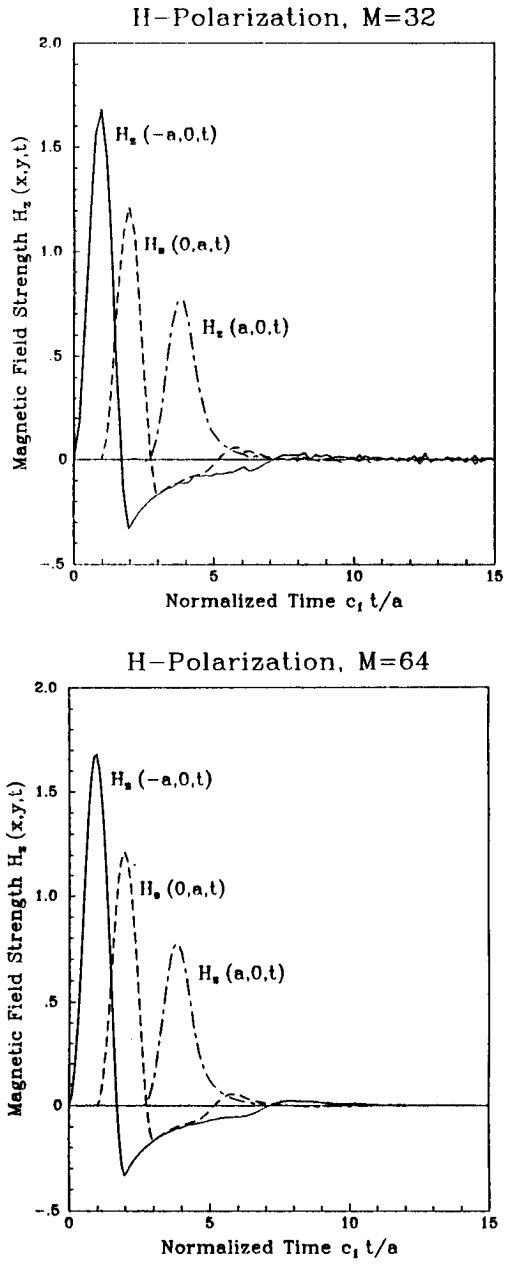


**Figure 13.3.2** $\mathcal{H}_z$ **as a function of normalized time for a perfectly conducting, circular cylinder of radius** $a$ **illuminated by an** $H$**-polarized sine-squared incident pulse of duration** $c_1T/a = 2$**. Discretization as indicated.**

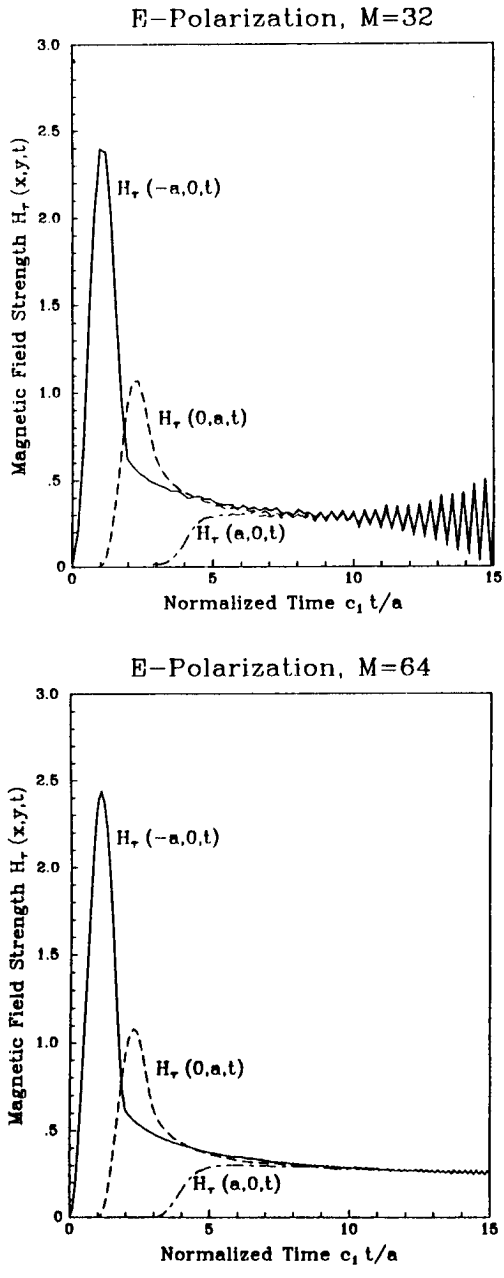


**Figure 13.3.3** $\mathcal{H}_\tau$ **as a function of normalized time for a perfectly conducting, circular cylinder of radius** $a$ **illuminated by an** $E$**-polarized sine-squared incident pulse of duration** $c_1 T/a = 2$**. Discretization as indicated.**

$t$, it turns out to be constant around the contour, and almost constant in time. Mathematically, this behavior can be explained by analyzing the scattering problem at hand with the aid of the Singularity Expansion Method [50]. The late-time behavior observed in Fig. 13.3.3 corresponds with the contribution from a branch-cut in the complex-frequency plane ending at $s = 0$. From a physical point of view, the incident field excites a "stationary" current propagating in the $z$-direction, and a corresponding "stationary" magnetic field around the cylinder. Both from mathematical (Riemann-Lebesgue) and from physical (energy) arguments, it follows that this contribution vanishes gradually as $t \to \infty$.

Because of this systematic behavior, the marching-on-in-time solution shown in Fig. 13.3.3 exhibits a systematic instability, whose start coincides with the onset of the "stationary" field. Comparing the results for $M = 32$ and $M = 64$ confirms the conjecture made above that even systematic instabilities may be controllable via the mesh size $h$. Additional confirmation is obtained from the fact that a similar computation with $M = 128$ produced completely stable results.

A more elegant solution to the special instability problem observed in Fig. 13.3.3 is to adapt the problem formulation such that the quantity to be computed does not exhibit the systematic behavior. This is achieved by computing $\partial_t \mathcal{H}_\tau(\rho, t)$ rather than $\mathcal{H}_\tau(\rho, t)$ itself. The relevant integral equation is obtained from (13.2.56) when both the incident field $\mathcal{H}^i_\tau(\rho .t)$ and the total field $\mathcal{H}_\tau(\rho, t)$ are replaced by their time derivatives. The field $\mathcal{H}_\tau(\rho, t)$ is then obtained by numerically integrating with respect to $t$. This scheme produces results with a similar stability behavior as observed in Fig. 13.3.2.

A possible disadvantage of the marching-on-in-time method is the sharp increase in computation time upon reduction of $h$. In a single computation, we must evaluate, at $\mathcal{O}(M)$ instants, at $M$ space points, $\mathcal{O}(M)$ different time integrals, each of which requires a weighted summation of $\mathcal{O}(M)$ field values. As a result, the number of operations is approximately proportional to $M^4$ as $M$ becomes large. For the fields shown in Fig. 13.3.2 and 13.3.3, the computation times were 54, 690 and 9900 seconds for $M = 32$, 64 and 128, respectively.

*Impenetrable Three-Dimensional Objects*

The situation for the magnetic-field integral equation for scattering by a three-dimensional, electrically impenetrable obstacle (13.2.52)

resembles the one described above. With the estimate (13.2.54), it follows directly that the coefficients $\tilde{k}(\alpha, \alpha', n - n')$ consist of a factor of $\mathcal{O}(h^2)$ from the two-dimensional space integration, and at worst at factor of $\mathcal{O}(h^{-1})$ from either the time differentiation or the extra factor of $R^{-1}$. This means that $\tilde{k}(\alpha, \alpha', n - n') = \mathcal{O}(h)$ as $h \to 0$. As in the case of the impenetrable cylinder, therefore, we expect only "systematic" instabilities that can be controlled by reducing the mesh size $h$.

To understand the nature of the "systematic" instabilities, we must be aware that the integral equation (13.2.52) has homogeneous solutions corresponding to the so-called "interior resonances" of the obstacle [51]. The corresponding resonant frequencies are located on the imaginary $s$-axis. Consequently, any homogeneous solution to (13.2.52) extends over the entire $t$-axis. From an analytical point of view, such solutions are eliminated by the initial condition that $\mathcal{H}(\mathbf{r}, t) = \mathbf{0}$ for $\mathbf{r} \in \partial\mathcal{D}$ and $-\infty < t \leq 0$. From a computational point of view, however, such solutions may cause problems when the space-time discretization leading to (13.3.3) shifts one or more of the resonant frequencies into the right half of the complex $s$-plane or, equivalently, outside the unit circle in the complex $z$-plane. In that case, the discretization introduces an instability with an unwanted "systematic" behavior.

Confirmation of these observations is readily available in the literature. The first numerical results for scattering by three-dimensional, electrically impenetrable targets were obtained by Bennett [9]. Rynne [30] verified for the case of a perfectly conducting sphere that reducing the mesh size removes the instabilities. In the same paper, he established the effectiveness of doubling the time step in the discretized time derivative. In a subsequent paper [44], Rynne actually reported the occurrence of oscillatory instabilities with the correct resonant frequencies. Recently, Smith [52,53] even recovered the spatial distribution of interior solutions to (13.2.52) from the exponentially increasing parts of unstable time-marching results.

These observations indicate that it should be possible, as in the case of the impenetrable cylinder, to adapt the problem formulation such that the "systematic" instabilities are avoided. In particular, it would be interesting to combine the magnetic-field integral equation (13.2.52) with the electric-field integral equation mentioned in Subsection 13.2.3. For the corresponding frequency-domain problem, such a

combined equation has no interior resonances [51]. The author is not aware of any pertinent time-domain results.

As in the previous two cases, we estimate the number of operations involved in applying the marching-on-in time method. Let $M$ be the number of space steps across a characteristic dimension of the obstacle. Then, we need to carry out, for $\mathcal{O}(M)$ instants, space integrations for $\mathcal{O}(M^2)$ space points, each of which requires a weighted summation of $\mathcal{O}(M^2)$ field values. In total, this adds up to $\mathcal{O}(M^5)$ operations.

*Dielectric Cylinder*

Next, let us consider the dielectric cylinder specified in connection with (13.2.64). For simplicity, we restrict ourselves to the case where the cylinder is embedded in free space, i.e. $\epsilon_1 = \epsilon_0$. For this configuration, we distinguish between two situations. For a nonvanishing susceptibility $\chi(\boldsymbol{\rho}) \stackrel{\text{def}}{=} \epsilon_{2r}(\boldsymbol{\rho}) - 1$, the approximate field values obtained are multiplied by a factor of $\mathcal{O}(h^{-2})$ due to the double time differentiation. In the singular part of the integrand, the product of the resulting approximation and the factor of $\ln(R/a)$ in (13.2.65) is integrated over a patch with sides of length $\mathcal{O}(h)$. For the point of observation and neighboring space-time points, this logarithmic term dominates the integrand of (13.2.64). This implies that we have the interpretation of Table 13.3.1, and that the weighting factors $w_0$ and $w_1$ are of $\mathcal{O}[\ln(h)]$. Hence, $w_0$ and $w_1$ will increase when $h$ is reduced. In view of this estimate, we should actually expect to introduce instabilities by refining the discretization.

A different situation arises when $\chi(\boldsymbol{\rho})$ vanishes in $\mathcal{D}_2$. In that case, we need only carry out a single time differentiation. Consequently, the weighting factors are at most of $\mathcal{O}[h\ln(h)]$, which suggests a stability behavior similar to that observed for the impenetrable cylinder.

To illustrate these considerations, we present in Figs. 13.3.4 and 13.3.5 results for the scattering of a Gaussian pulse of duration $c_0T/a = 10$ by a homogeneous, square cylinder of width $2a$, centered around the origin. The spatial mesh is simple cubic, with $h = a/M$. Figure 13.3.4 pertains to the case where $\chi(\boldsymbol{\rho}) = 0$. The value of the dimensionless conductivity was chosen such that the marching-on-in-time results obtained by using a single-step difference rule for the time derivative are just unstable. This result is displayed in the upper left corner. Note that the alternating, unstable component of the solution that shows up for $c_0t/a > 15$ moves in the same direction across the

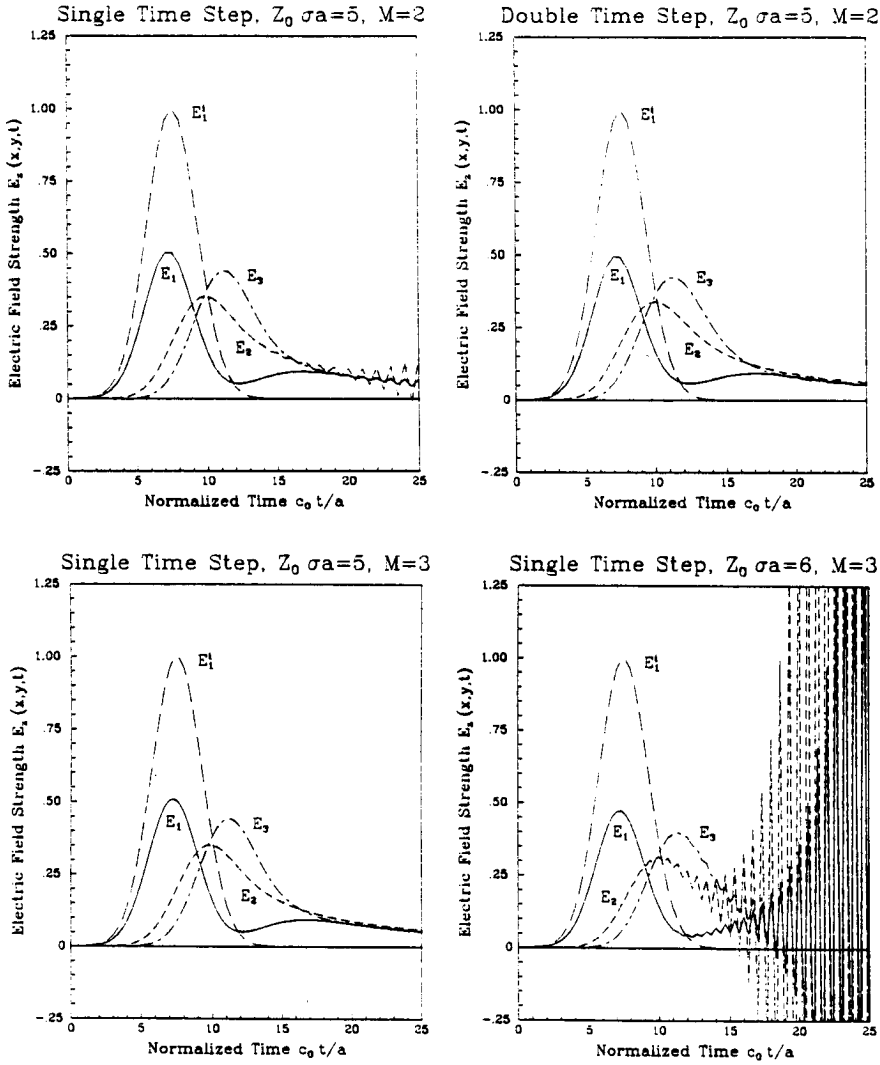


**Figure 13.3.4 Results of applying the marching-on-in-time method to obtain the field excited in a homogeneous square cylinder of width $2a$, with $\chi = 0$. Point 1 $= (-a, 0)$, Point 2 $= (0, 0)$, Point 3 $= (a, 0)$. Conductivity and discretization as indicated in the figure headings.**

entire cylinder. Moreover, the start of the unstable behavior coincides in time with the onset of a "stationary" behavior of the actual field, which corresponds to the excitation of an almost constant, "stationary" current distribution across the cylinder. The remaining results in Fig. 13.3.4 indicate a limited success of doubling the time step and of refining the discretization. This confirms the interpretation of the instability as a systematic one: both measures will mainly take effect when the discretized integral is dominated by the contributions from a few space-time points near the point of observation.

The results of applying the marching-on-in-time method to the problem of transient scattering by a cylinder with only a susceptibility contrast are even more discouraging. For the discretization with a single step in the backward difference rule for the second-order time derivative, the stability range is not worth mentioning. When the double time step is used, and the discretization is not too fine, stable results can be obtained until at most $\chi = 2$. As predicted above, however, refining the discretization may stir up the instabilities again. An example is given in Fig. 13.3.5, which shows, for the same configuration, a stable result obtained for $M = 2$ and an unstable result obtained for $M = 3$. In the lower part of Fig. 13.3.5, it is observed that, due to the choice of the double time step, the unstable part of the marching-on-in-time result no longer changes sign at each new instant. Instead, we have an interplay of instabilities that alternate with the double time step, as mentioned towards the end of Subsection 13.3.3.

For the dielectric cylinder, the computation of a single time-domain result entails, at $\mathcal{O}(M)$ instants, the evaluation at $\mathcal{O}(M^2)$ space points of $\mathcal{O}(M)$ different time integrals, each of which requires a weighted summation of $\mathcal{O}(M)$ field values. Once these time integrals have been determined, $\mathcal{O}(M^2)$ space integrals must be computed, each of which, in turn, requires a weighted summation of $\mathcal{O}(M^2)$ time integrals. Finally, the multiplication with an inverted weigthing matrix as outlined in (13.3.5) requires $\mathcal{O}(M^4)$ operations. As a result, the total effort is of $\mathcal{O}(M^5)$. For the fields shown in Fig. 13.3.4, for example, the computation times for M=2, 3 and 4 were 14, 78 and 278 seconds, respectively. Especially the relation between the computation times for M=3 and M=4 is in good agreement with the estimate that the computational effort is of $\mathcal{O}(M^5)$.

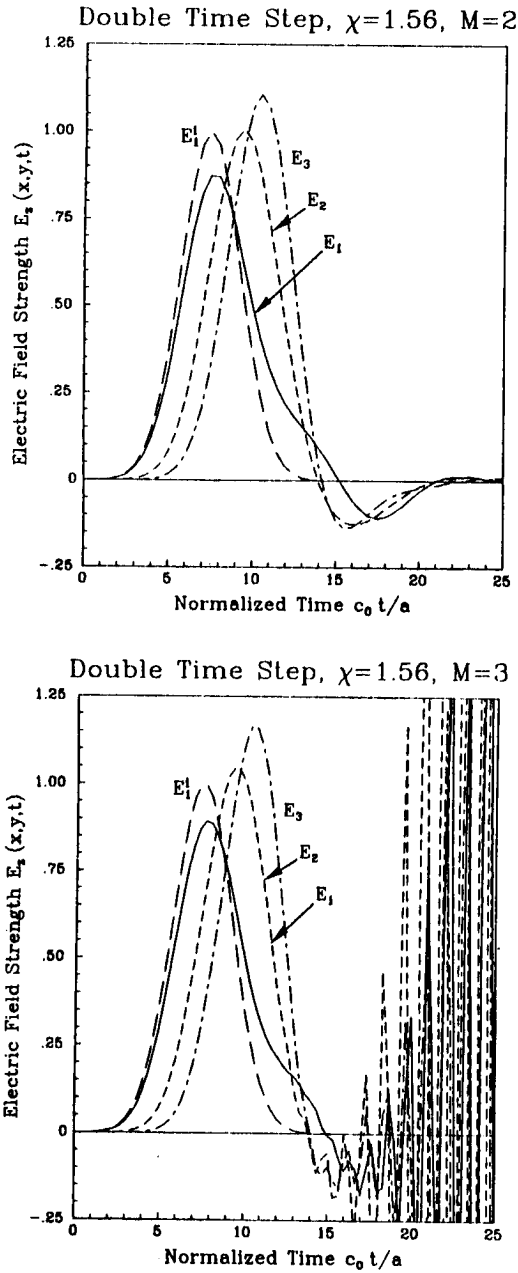


**Figure 13.3.5 Results of applying the marching-on-in-time method to obtain the field excited in a homogeneous, lossless square cylinder with $\chi = 1.56$. Point 1 = $(-a, 0)$, Point 2 = $(0, 0)$, Point 3 = $(a, 0)$. Discretization as indicated in the figure headings.**

## 13.4 The Conjugate-Gradient Method

The results presented in Subsection 13.3.5 illustrate that solving integral equations of the type (13.3.1) with the aid of the marching-on-in-time method may not always be feasible. In particular, the sharp increase in computation time makes it unacceptable to refine the space-time discretization much further than required by the physics of the problem merely for the sake of stabilizing a numerical algorithm. In addition, we have demonstrated the existence of cases where reducing $h$ may be ineffective, or even counterproductive.

One way to avoid these problems is to leave the, supposedly accurate, discretization as is, and to solve (13.3.3) by a different method of solution. Short of transforming that equation to the frequency-domain, which may actually be more efficient than it seems [49], the only option appears to be using iterative techniques. In the remainder of this chapter, we discuss two possible procedures. In Section 13.5, we propose a relaxation method taylored to the special nature of the instabilities derived in Subsection 13.3.3. In the present section, we consider how the conjugate-gradient method can be employed.

### *13.4.1 Formulation of the Method*

Let us first cast the conjugate-gradient method into the framework of the operator formulation introduced in Subsection 13.2.5. Following the notation of Dudley [54] and Van den Berg [55], we start by introducing the inner product of two space-time field quantities $u(\mathbf{r},t)$ and $v(\mathbf{r},t)$ over the domain $\mathcal{D}$ figuring in (13.3.1) as

$$\langle u,v\rangle \stackrel{\text{def}}{=} \int_{\mathcal{D}} d\mathbf{r} \int_{-\infty}^{\infty} dt\, u(\mathbf{r},t)v(\mathbf{r},t) \tag{13.4.1}$$

In (13.4.1), the product of $u$ and $v$ at the space-time point $\{\mathbf{r},t\}$ is regarded as a vector inner product when appropriate. Since we are dealing with time-domain fields, complex conjugations are not necessary. With this inner product, we associate the norm:

$$||u|| \stackrel{\text{def}}{=} \langle u,u\rangle^{\frac{1}{2}} \tag{13.4.2}$$

Further, we define the Hermitean adjoint $L^\star$ of an operator $L$ as that operator for which

$$\langle Lu,v\rangle = \langle u,L^\star v\rangle \tag{13.4.3}$$

for all $u$ and $v$ in the space of possible solutions of the integral equation (13.3.1).

Referring to that integral equation, let $u^{app}$ be an approximate solution. Then, we define the corresponding residual or equation error as

$$r \stackrel{\text{def}}{=} Lu^{app} - f \tag{13.4.4}$$

and the normalized root-mean-square error ERR as

$$\text{ERR} \stackrel{\text{def}}{=} ||r||/||f|| \tag{13.4.5}$$

Following Van den Berg [32,33], we now introduce a sequence of expansion functions $\{\phi_j(\mathbf{r},t) \mid j = 1,\ldots,\infty\}$ that belong to the same Hilbert space as the unknown solution $u(\mathbf{r},t)$. With the aid of these expansion functions, we construct successive approximations $\{u_j(\mathbf{r},t)\}$ to the actual solution $u(\mathbf{r},t)$. Ideally, we would like to construct each iterate $u_j(\mathbf{r},t)$ such that the corresponding residual error $r_j(\mathbf{r},t)$ minimizes the root-mean-square error defined in (13.4.5) for any choice of $\{\phi_j\}$. However, this would involve storing $j$ space-time domain functions in memory, as well as the results of applying the operator $L$ to these functions [55].

Since, for time-domain problems, such a scheme would hardly be practical, we restrict ourselves to a scheme in which we need to store simultaneously

- a single expansion function $\phi_j(\mathbf{r},t)$,
- a single correction function $u_j^{cor}(\mathbf{r},t)$,
- the result of applying the operator $L$ to both these functions,
- the previous approximation $u_{j-1}(\mathbf{r},t)$ and the corresponding residual $r_{j-1}(\mathbf{r},t)$.

For a general choice of the expansion functions $\{\phi_j\}$, we start the iterative procedure by choosing

$$\begin{aligned} u_0 &= 0 \\ r_0 &= -f \\ \text{ERR}_0 &= \|-f\| \,/\, \|f\| = 1 \end{aligned} \tag{13.4.6}$$

Next, we define the "search direction" [56]. For $j = 1$, we choose the correction function as

$$\begin{aligned} u_1^{cor} &= \phi_1 \\ Lu_1^{cor} &= L\phi_1 \end{aligned} \tag{13.4.7}$$

For $j \geq 2$, we take

$$\begin{aligned} \xi_j &= \langle L u_{j-1}^{cor}, L\phi_j \rangle / B_{j-1} \\ u_j^{cor} &= \phi_j - \xi_j u_{j-1}^{cor} \\ L u_j^{cor} &= L\phi_j - \xi_j L u_{j-1}^{cor} \end{aligned} \tag{13.4.8}$$

In each iteration step we then correct $u$ in the direction of $u_j^{cor}$. This amounts to carrying out an "exact line search" [56]. For $j = 1, 2, \ldots, \infty$, we compute

$$\begin{aligned} A_j &= \langle L u_j^{cor}, r_{j-1} \rangle \\ B_j &= ||L u_j^{cor}||^2 \\ \alpha_j &= -A_j / B_j \\ u_j &= u_{j-1} + \alpha_j u_j^{cor} \\ r_j &= r_{j-1} + \alpha_j L u_j^{cor} \\ \mathrm{ERR}_j &= ||r_j|| / ||f|| \end{aligned} \tag{13.4.9}$$

In (13.4.8) and (13.4.9), $\xi_j$, $A_j$, $B_j$ and $\alpha_j$ are real-valued constants.

The effectiveness of the scheme outlined above depends strongly on the possibility of generating suitable expansion functions $\{\phi_j\}$. Various possibilities can be found in [33,55]. In the present context, we restrict ourselves to the choice made in the *conjugate-gradient method*:

$$\phi_j \overset{\text{def}}{=} L^* r_{j-1} \tag{13.4.10}$$

For this choice, the expansion function $\phi_j$ is the so-called gradient direction, and the correction function $u_j^{cor}$ the conjugate-gradient direction. Owing to a number of orthogonality properties [33], we reach, at least theoretically, even the purpose set above of minimizing $||r_j||$ in each iteration step.

The same orthogonality properties also lead to a simplification of the iterative scheme. The first step remains as specified in (13.4.6), i.e.

$$\begin{aligned} u_0 &= 0 \\ r_0 &= -f \\ \mathrm{ERR}_0 &= 1 \end{aligned} \tag{13.4.11}$$

As stated above, we choose the expansion functions in the gradient direction

$$\begin{aligned} \phi_j &= L^* r_{j-1} \\ A_j &= ||\phi_j||^2 \end{aligned} \tag{13.4.12}$$

for $j = 1, 2, \ldots, \infty$. From these expansion functions, we determine the correction functions according to

$$\begin{aligned} u_1^{cor} &= \phi_1 && \text{for } j = 1 \\ u_j^{cor} &= \phi_j + (A_j/A_{j-1})\, u_{j-1}^{cor} && \text{for } j \geq 2 \end{aligned} \tag{13.4.13}$$

The update step (13.4.9) now reduces to computing, for $j = 1, 2, \ldots, \infty$,

$$\begin{aligned} B_j &= ||Lu_j^{cor}||^2 \\ \alpha_j &= -A_j/B_j \\ u_j &= u_{j-1} + \alpha_j\, u_j^{cor} \\ r_j &= r_{j-1} + \alpha_j\, Lu_j^{cor} \\ \text{ERR}_j &= ||r_j||/||f|| \end{aligned} \tag{13.4.14}$$

Compared with the original iteration scheme given in (13.4.9), this saves, in each iteration step, the computation of the inner products $\langle Lu_{j-1}^{cor}, L\phi_j \rangle$ and $\langle Lu_j^{cor}, r_{j-1} \rangle$.

Most of the computational effort will be spent in evaluating $L^\star r_j$ and $Lu_j^{cor}$. For a given discretization, each of these computations takes at least as much effort as carrying out a complete marching-on-in-time computation. This need not keep us from applying the method, however: doubling the discretization to obtain a stable time-marching result also increases the computational effort by a factor of 16 or 32, which is equivalent to performing 8 or 16 iteration steps in the conjugate-gradient method for the original discretization.

### *13.4.2 The Adjoint Operator*

The reason that the conjugate-gradient method does not encounter the instabilities introduced in the discretized integral equation (13.3.3) is that this method inherently imposes the restriction that $\langle u_j, u_j \rangle$ exists for each $j$. With (13.4.1), this implies that the successive approximations $\{u_j(\mathbf{r}, t)\}$ are square integrable in time, and, consequently, decrease in magnitude as $t \to \infty$. On the other hand, this restriction excludes cases where the unknown field approaches an almost constant value at late times, as displayed in Figs. 13.3.3 and 13.3.4. In such cases, however, we can resort to solving for $\partial_t u(\mathbf{r}, t)$ instead, as mentioned in connection with Fig. 13.3.3.

The above explanation can be clarified further by considering the structure of the adjoint operator $L^\star$. With (13.2.69) and (13.4.3), we directly have

$$L^\star = I - K^\star \tag{13.4.15}$$

where $K^\star$ is defined on the scattering domain only. Using the additional information contained in (13.2.70) and (13.2.71), we find

$$K^\star u(\mathbf{r},t) = \sum_{p=0}^{P} C_p^T(\mathbf{r}) \int_{\mathcal{D}} d\mathbf{r}' \int_{t+R/c}^{\infty} dt'\, g_p(R,t'-t)\,(-\partial_{t'})^p\, u(\mathbf{r}',t') \tag{13.4.16}$$

where the superscript $T$ indicates that the transpose of $C_p(\mathbf{r})$ is to be taken when appropriate. By replacing $t \rightarrow -t$, (13.4.16) can be rewritten as

$$K^\star u(\mathbf{r},-t) = \sum_{p=0}^{P} C_p^T(\mathbf{r}) \int_{\mathcal{D}} d\mathbf{r}' \int_{-\infty}^{t-R/c} dt'\, g_p(R,t-t')\,(\partial_{t'})^p\, u(\mathbf{r}',-t') \tag{13.4.17}$$

which, apart from the position of the configuration parameter $C_p^T(\mathbf{r})$, has the same structure as the "forward" operator $K$ specified in (13.2.70) and (13.2.71).

Now, let the "forcing function" $f(\mathbf{r},t)$ correspond to an incident pulse of finite duration $T$. For $\mathbf{r} \in \mathcal{D}$, we then have $f(\mathbf{r},t) = 0$ outside a finite time interval $0 < t < T_{max}^{(0)}$. By (13.4.11), the residual $r_0(\mathbf{r},t)$ is then confined to the same time interval. With either (13.4.16) or (13.4.17) and the properties of $g_p(R,t)$ derived in Subsection 13.2.2, this leads to the conclusion that $\phi_1(\mathbf{r},t)$ vanishes or becomes negligible outside a finite time interval $T_{min}^{(1)} < t < T_{max}^{(0)}$. By (13.4.14), we then have the same time limitation for the first iterate $u_1(\mathbf{r},t)$. Finally, with (13.2.70) and (13.2.71), it follows that $r_1(\mathbf{r},t)$ vanishes or becomes negligible outside a finite time interval $T_{min}^{(1)} < t < T_{max}^{(1)}$, which brings us back to the starting point of a time-limited residual.

Repeating the argument, therefore, we find that, for $\mathbf{r} \in \mathcal{D}$, each successive approximation $u_j(\mathbf{r},t)$ vanishes or becomes negligible outside a time interval $T_{min}^{(j)} < t < T_{max}^{(j-1)}$, with $T_{min}^{(j)} \leq T_{min}^{(j-1)} \leq 0$ and $T \leq T_{max}^{(j-1)} \leq T_{max}^{(j)}$. This explains why the iterates can only converge to a time-limited solution $u(\mathbf{r},t)$.

Furthermore, the analysis given above reveals that, in the implementation, we need to exercise special care in selecting the time

interval under consideration. In the marching-on-in-time method, we simply start the computation at $t = 0$, and terminate it at will. In the conjugate-gradient method, we must ensure that the computation extends far enough in both the negative and the positive time directions to accomodate the successive residuals and correction functions.

*Discretization Aspects*

The feature of the iterative scheme outlined in (13.4.11)–(13.4.14), that both operators $L$ and $L^\star$ are only applied to *known* space-time functions resulting from the previous iteration step, gives us more freedom in discretizing the time derivatives. For example, we can replace (13.3.15) by the two-term central difference rule

$$\partial_{t'} u(\mathbf{r}', t') = \left[u(\mathbf{r}', t' + \Delta t) - u(\mathbf{r}', t' - \Delta t)\right] / 2\Delta t \tag{13.4.18}$$

or by the three-term forward difference rule

$$\partial_{t'} u(\mathbf{r}', t') = \left[-\frac{3}{2}u(\mathbf{r}', t') + 2u(\mathbf{r}', t' + \Delta t) - \frac{1}{2}u(\mathbf{r}', t' + 2\Delta t)\right] / \Delta t \tag{13.4.19}$$

both of which are based on quadratic time interpolation and hold up to $\mathcal{O}(\Delta t^2)$ [46]. Neither of these approximations is useful in the marching-on-in-time method, where we only have the field values $\{\tilde{u}(\alpha', n') \mid n' < n\}$ at our disposal when $\tilde{u}(\alpha, n)$ is determined.

A possible consequence of discretizing both operators is that, even with the choice of $\{\phi_j\}$ made in (13.4.10), the schemes given in (13.4.6)–(13.4.9) and (13.4.11)–(13.4.14) may not be equivalent. The equivalence of both schemes is conserved if and only if the discretized adjoint operator $\tilde{L}^\star$ is matrix adjoint to the discretized operator $\tilde{L}$. To clarify this, let us consider $\tilde{L}$. From (13.3.3), we observe that

$$\tilde{L}\tilde{u}(\alpha, n) = \tilde{u}(\alpha, n) - \sum_{\alpha'} \sum_{n'=-\infty}^{n} \tilde{k}(\alpha, \alpha'; n - n')\tilde{u}(\alpha', n') \tag{13.4.20}$$

for $n \in \mathbb{Z}$. The discretized equivalent of the inner product (13.4.1) is of the form

$$\langle \tilde{u}, \tilde{v} \rangle \stackrel{\text{def}}{=} \Delta t \sum_{\alpha} w_\alpha \sum_{n=-\infty}^{\infty} \tilde{u}(\alpha, n)\tilde{v}(\alpha, n) \tag{13.4.21}$$

where $w_\alpha$ denotes a scalar weighting coefficient that originates from the integration over $\mathcal{D}$ in (13.4.1).

Defining the adjoint discretized operator $\tilde{L}^\star$ in analogy with (13.4.3), we find

$$\tilde{L}^\star \tilde{u}(\alpha,n) \stackrel{\text{def}}{=} \tilde{u}(\alpha,n) - \sum_{\alpha'} \frac{w_{\alpha'}}{w_\alpha} \sum_{n'=n}^{\infty} \tilde{k}(\alpha',\alpha;n'-n)\tilde{u}(\alpha',n') \quad (13.4.22)$$

Among other things, (13.4.22) implies that forward differences should be used to approximate the time differentiations occurring in $L^\star$ when backward differences are used for $L$, and vice versa. Alternatively, central differences can be employed in the discretization of both operators.

Deviating from (13.4.22) means that the convergence of the conjugate-gradient procedure specified in (13.4.11)–(13.4.14) is no longer guaranteed. This can be explained from the fact that the orthogonality relations needed to reduce (13.4.6)–(13.4.9) to (13.4.11)–(13.4.14) rely on the property that $\tilde{L}$ and $\tilde{L}^\star$ are adjoint with respect to the discretized inner product (13.4.21). The original scheme (13.4.6)–(13.4.9), which was derived for "arbitrary" expansion functions $\{\phi_j\}$, will remain convergent even when (13.4.22) is violated. An illustrative example will be presented below, in Subsection 13.4.4.

As far as the time discretization is concerned, we can automatically attain the form (13.4.22) by utilizing the time-reversed expression (13.4.17). This means that the marching-on-in-time code, which should constitute the core of any implementation of a time-domain iterative scheme, must be expanded by a time-reversal subroutine, and not by one for evaluating the adjoint operator.

Finally, the above exercises with the discretization raise the question to what extent the discretized operators determine the eventual result if the iterative scheme converges. The answer is implied in the definition of the errors $r$ and ERR in (13.4.4)–(13.4.5): the final result depends primarily on the discretized "forward" operator $\tilde{L}$. Only having $\tilde{L}\tilde{u} - \tilde{f} = 0$ can make the norm of the type (13.4.2) associated with the discretized inner product (13.4.21) vanish. As long as that norm differs from zero, the application of the adjoint operator according to (13.4.10) will continue to generate nonvanishing expansion functions $\phi_j(\alpha,n)$.

In particular, this observation leads to an interesting conclusion for cases where the marching-on-in-time method does not suffer from instabilities: applying either of the iterative schemes (13.4.6)–(13.4.9)

or (13.4.11)–(13.4.14) with the time derivatives in $L$ approximated by backward differences will converge to precisely that result for which the error in the equality sign in (13.3.3) vanishes, i.e. the time-marching solution. This will be demonstrated in Subsection 13.4.4 as well.

### *13.4.4 Examples*

To illustrate the special properties of applying the conjugate-gradient method to transient-scattering problems, we reconsider the "tutorial" example of plane-wave scattering by a dielectric slab as specified in Subsection 13.2.4. Strictly speaking, we need not solve the integral equation (13.2.67) iteratively, since the marching-on-in-time method is capable of solving this equation up to any desired accuracy. However, it is convenient to consider a configuration for which the exact solutions to both the continuous and the discretized integral equations are available.

In Figure 13.4.1, we show the influence of the manner in which the operators $L$ and $L^\star$ are discretized. In particular, we vary the discretization of the time derivatives as discussed in connection with Equations (13.3.15), (13.4.18) and (13.4.19). For the lossless, homogeneous slab considered in Fig. 13.3.1 and Table 13.3.3, we have applied the conjugate-gradient method as given in (13.4.11)–(13.4.14) in four different versions:

A: Using the backward difference rule (13.3.15) for the time derivative in $\tilde{L}$, and the forward difference rule (13.4.19) for the time derivative in $\tilde{L}^\star$.

B: Using the backward difference rule (13.3.15) in $\tilde{L}$, and the central difference rule (13.4.18) in $\tilde{L}^\star$.

C: Using the central difference rule (13.4.18) in $\tilde{L}$, and the forward difference rule (13.4.19) in $\tilde{L}^\star$.

D: Using the central difference rule (13.4.18) in both operators $\tilde{L}$ and $\tilde{L}^\star$.

Only for versions A and D is $\tilde{L}^\star$ adjoint to $\tilde{L}$ in the sense of (13.4.22). From Fig. 13.4.1, it is observed that the conjugate-gradient method converges for precisely those two versions. For Version B, the convergence stalls, and for Version C the successive iterates even diverge.

The numerical experiment of Fig. 13.4.1 was repeated for the original iterative scheme specified in (13.4.6)–(13.4.9). Now, all four versions converged. Versions A and D converged at the same rate as in

Fig. 13.4.1, Version B was slightly slower than Version A, and Version C was about two times slower.

These results confirm the conclusion drawn in connection with (13.4.22), that the convergence of the reduced scheme (13.4.11)–(13.4.14) can only be guaranteed when the adjoint operator $L^\star$ is discretized such that $\tilde{L}^\star$ is adjoint to $\tilde{L}$ with respect to the discretized inner product (13.4.21).

This effect is not an artifact due to the choice of too coarse a mesh: for the present discretization, the root-mean-square error introduced in Table 13.3.3 was 2.01% and 1.04% for the marching-on-in-time result and for the "final" result of Version D, respectively. Nevertheless, both the schemes (13.4.6)–(13.4.9) and (13.4.11)–(13.4.14) were also tested for a finer space-time discretization, i.e. a larger $M$, with similar results. The main difference was that the overall rate of convergence slowed down, and that Version C started to diverge at a smaller value of the root-mean-square error. Independently of $M$, the root-mean-square error $||\tilde{\mathcal{E}}_z - \mathcal{E}_z||/||\mathcal{E}_z||$ obtained with central difference rules was about a factor of 2 smaller than the one obtained by using a backward rule in $\tilde{L}$.

The numerical experiments described above also give an indication for the optimal choice between the finite-difference rules (13.3.15), (13.4.18) and (13.4.19). As far as the discretization error is concerned, these rules seem almost interchangeable. Therefore, we can choose whichever one is most appropriate for the numerical computation at hand. In the marching-on-in-time method, this would be the backward rule (13.3.15), which is the only one admissible in the "self term". In the conjugate-gradient method, this would be the central rule (13.4.18) because it leads to a faster convergence.

Selecting Version D, therefore, we investigate in Figs. 13.4.2–13.4.4 the effect of varying some of the numerical and physical parameters. In Fig. 13.4.2, we show the effect of refining the space-time mesh. In Figures 13.4.3 and 13.4.4, the influence of varying the permittivity of the slab and the duration of the incident pulse is demonstrated.

All of these figures confirm the matrix interpretation of the discretized integral equation (13.3.3) leading to the error analysis of Subsections 13.3.2 and 13.3.3 , and to the definition of the discretized adjoint operator $\tilde{L}^\star$ in Subsection 13.4.3. Recall that (13.3.3) can be envisaged as an essentially lower-triangular matrix equation whose system matrix has a large number of "well-behaved" eigenvectors corre-

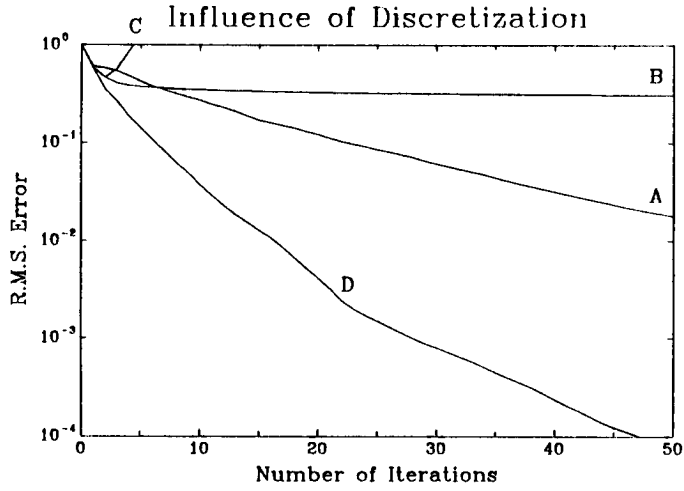


**Figure 13.4.1 Convergence of four different realizations of the conjugate-gradient method as specified in the text. The configuration is a homogeneous, lossless dielectric slab with $\epsilon_{2r} = 2.25$ in free space, excited by a sine-squared incident pulse of duration $c_0 T/d = 2$, subdivided in $M = 20$ subintervals.**

sponding to eigenvalues of $\mathcal{O}(1)$, and, possibly, a few "problematic" eigenvectors corresponding to small eigenvalues. Since each step of the conjugate-gradient method corrects the component along a single basis vector in the solution space of (13.3.3), the rate of convergence depends on the size of the subspace in which such corrections are necessary. Refining the space-time discretization obviously enlarges the number of eligible basis vectors. Increasing the permittivity of the slab introduces more "detail" in the space-time solution, in the form of repeatedly reflected and transmitted pulses with larger amplitudes, and necessitates an extension of the time interval under consideration. Shortening the pulse duration enhances the "detail" within a fixed time interval.

In view of this matrix interpretation, we cannot expect the value of the root-mean-square error to be indicative of the actual accuracy of the discretized solution $\tilde{u}_j(\alpha, n)$ obtained. The only information contained in this value is how well $\tilde{u}_j(\alpha, n)$ resembles the "exact" solution $\tilde{u}(\alpha, n)$ of the discretized equation (13.3.3). The effect of replacing the continuous equation (13.3.1) with its discretized counterpart (13.3.3) must be investigated separately. A confirmation of this observation was already obtained in Fig. 13.4.1, where the root-mean-square error

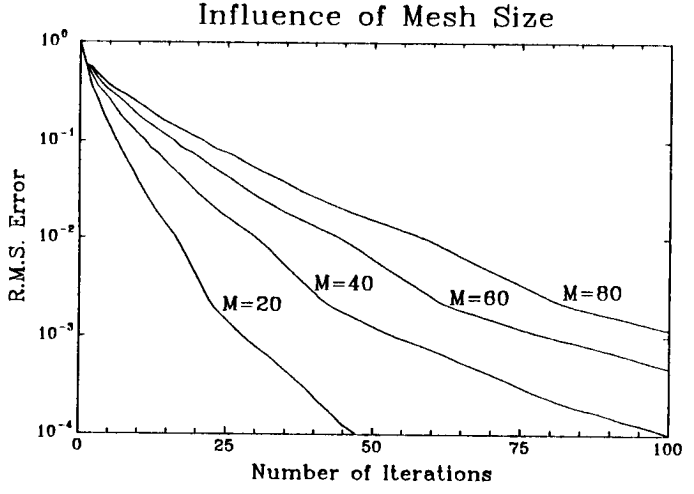


**Figure 13.4.2** Influence of the mesh size $h = d/M$ on the convergence of the conjugate-gradient method. The configuration is a homogeneous, lossless dielectric slab with $\epsilon_{2r} = 2.25$ in free space, excited by a sine-squared incident pulse of duration $c_0T/d = 2$.

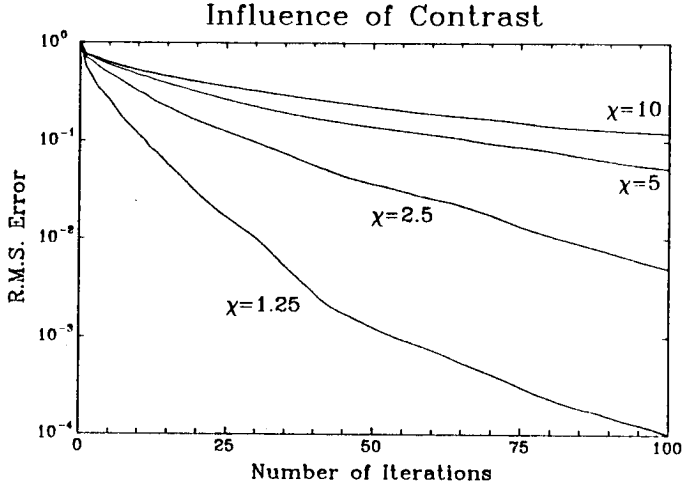


**Figure 13.4.3** Influence of permittivity contrast on the convergence of the conjugate-gradient method. The configuration is a homogeneous, lossless dielectric slab with $\epsilon_{2r} = 1 + \chi$ in free space, excited by a sine-squared incident pulse of duration $c_0T/d = 2$, subdivided in $M = 40$ subintervals.

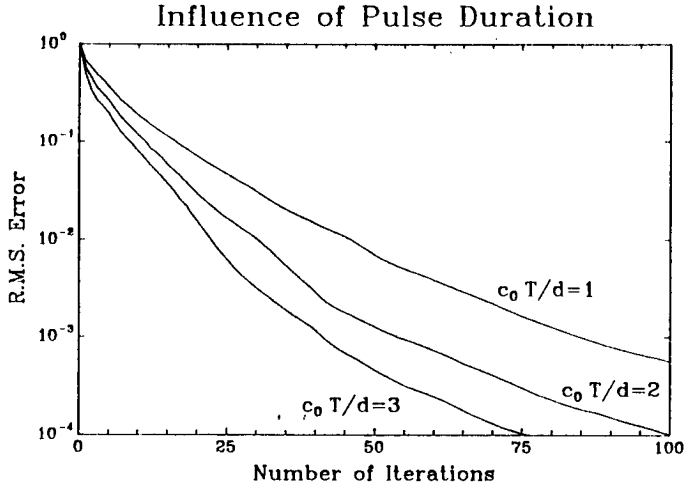


**Figure 13.4.4 Influence of pulse duration on the convergence of the conjugate-gradient method. The configuration is a homogeneous, lossless dielectric slab with $\epsilon_{2r} = 2.25$ in free space, excited by a sine-squared incident pulse of duration $c_0T/d$ as specified, and subdivided in $M = 40$ subintervals.**

reached by Version D was 0.007%, while actual error in the solution obtained was 1.04%. In addition, the result of carrying out 100 steps with Version A agreed up to four digits with the marching-on-in-time solution, as predicted towards the end of Subsection 13.4.3.

A special feature of the conjugate-gradient method is that, owing to its global nature, this method is able to handle domain integral equations with "negative velocity contrast" as analyzed in Subsection 13.3.4. A representative result is presented in Fig. 13.4.5. The configuration is a sine-squared pulse of duration $c_0T/d = 1$, incident on a homogeneous, lossless slab with $\epsilon_{2r} = 2.25$ embedded in a homogeneous, lossless dielectric with $\epsilon_{1r} = 6.25$. The result is about as accurate as the one displayed in the upper half of Fig. 13.3.1. The increase in the number of discretization steps from $M = 40$ to $M = 100$ is necessitated by the fact that the time sampling should be gauged with respect to the dimensionless pulse duration in the external medium, i.e. $c_1T/d = (\epsilon_{1r})^{-\frac{1}{2}} = 1/2.5 = 0.4$.

Finally, it should be remarked that, in the computations summarized in Figs. 13.4.1–13.4.5, convergence could only be obtained by considering a time interval that was at least twice as long as the

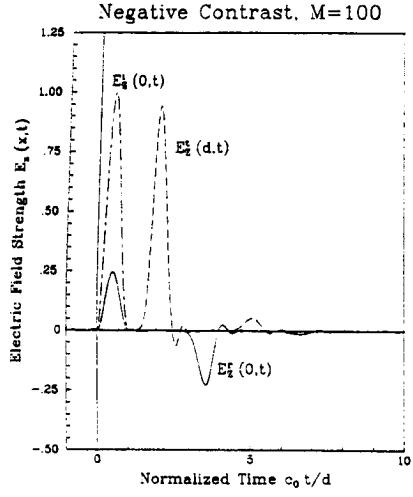


**Figure 13.4.5 Final result of carrying out 250 steps in the conjugate-gradient method for a homogeneous, lossless slab with $\epsilon_{2r} = 2.25$ embedded in a homogeneous, lossless dielectric with $\epsilon_{1r} = 6.25$, excited by a sine-squared incident pulse of duration $c_0T/d = 1$.**

one in which the true electric-field strength differs significantly from zero. This means that, in practice, each iteration step in the conjugate-gradient method requires an effort equivalent to performing four complete marching-on-in-time computations.

### *13.4.5 Rao's Approach*

In view of the large number of operations involved in applying the conjugate-gradient method to the full discretized integral equation (13.3.3), Rao et al. have proposed a different way to use this method for solving time-domain scattering problems [57]. The suggestion is to minimize the equation error in (13.3.3) successively at separate instants. For each $n$, the computation is terminated when the equation error reaches a suitably chosen value. In [57], this approach was applied successfully to the example of a perfectly conducting straight wire irradiated by a Gaussian electromagnetic pulse.

The effectiveness of Rao's approach can be understood from the matrix interpretation of (13.3.3) as well. The conjugate-gradient method has the tendency to first determine the components of $\tilde{u}_j(\alpha, n)$ along those eigenvectors of the system matrix that correspond to the

largest eigenvalues. By terminating the computation at the proper value of the equation error, therefore, it may be possible to reach the correct components along the "well-behaved" eigenvectors corresponding to eigenvalues of $\mathcal{O}(1)$, while avoiding unwanted components along the "problematic" ones corresponding to small eigenvalues. Continuing the computation too long will, of course, yield the exact solution of (13.3.3), i.e. the unstable marching-on-in-time result that we want to avoid.

Rao's approach is only applicable when the spatial distribution of the unstable part of $\tilde{u}_j(\alpha, n)$ differs significantly from the true field distribution at each instant. An example where this condition is violated is the impenetrable circular cylinder considered in Figs. 13.3.2 and 13.3.3. From Figure 13.3.3, in particular, it is observed that both the true field at late times and the unstable part of the time-marching solution are constant all around the cylinder boundary.

For this configuration, it follows from (13.2.56), (13.2.57), and the relevant estimate of the integrand as $R \to 0$, that

$$w(\alpha, \alpha') = \left(1 \pm \frac{1}{M}\right) \delta_{\alpha\alpha'} \tag{13.4.23}$$

where $w(\alpha, \alpha')$ denotes the weighting matrix introduced in (13.3.4). In (13.4.23), the $+$ and $-$ signs refer to the cases of magnetically and electrically polarized incident fields, respectively. The conjugate-gradient method inverts the weighting matrix $w(\alpha, \alpha')$ in a single step. For this configuration, therefore, Rao's approach will produce exactly the same results as the marching-on-in-time method.

## 13.5 The Relaxation Method

In this section, we describe a second iterative method that is capable of determining a stable solution to the discretized integral equation (13.3.3). In this so-called *relaxation method*, which was first presented in [37, Section 3.2], we combine the best ideas of the marching-on-in-time approach and of the conjugate-gradient method. In particular, we use the lower-triangular structure of the discretized integral equation as well as the concept of minimizing a squared error. By combining both ideas, we arrive at a relatively efficient, inherently stable scheme for solving the discretized integral equation (13.3.3).

*Formulation in Matrix Form*

Before we can actually apply the relaxation method, we must first derive it in a general form. To this end, we consider a system of $N$ linear equations for $N$ unknown variables $\{x_n\}$, components of a vector $\mathbf{x}$. This system can be written in matrix form as

$$\sum_{n=1}^{N} A_{mn}\, x_n = b_m \tag{13.5.1}$$

where $m = 1, 2, \ldots, N$. In (13.5.1), $A$ denotes the system matrix and $b_m$ is a component of a known vector $\mathbf{b}$. We assume the matrix $A$ to be nonsingular. In that case, $A$ has $N$ nonvanishing eigenvalues $\lambda_\ell$, $\ell = 1, 2, \ldots, N$, with $N$ corresponding eigenvectors $\mathbf{v}_\ell$.

Expanding both the unknown vector $\mathbf{x}$ and the known vector $\mathbf{b}$ in terms of these eigenvectors, we formally have

$$\mathbf{b} = \sum_{\ell=1}^{N} \beta_\ell\, \mathbf{v}_\ell \tag{13.5.2}$$

$$\mathbf{x} = \sum_{\ell=1}^{N} \xi_\ell\, \mathbf{v}_\ell = \sum_{\ell=1}^{N} \lambda_\ell^{-1}\, \beta_\ell\, \mathbf{v}_\ell \tag{13.5.3}$$

In (13.5.2), (13.5.3) and in the remainder of this subsection, we use Greek symbols to indicate the components along the eigenvectors $\{\mathbf{v}_\ell\}$. This notation is used to avoid confusion with the components in the original coordinate frame.

In the numerical solution of (13.5.1), problems can be expected when one of the eigenvalues $\{\lambda_\ell\}$ is small in magnitude. As (13.5.3) indicates, a small deviation in the known vector $\mathbf{b}$ along the corresponding eigenvector(s) may then cause a considerable error in the solution vector $\mathbf{x}$ obtained.

When the components of $\mathbf{x}$ along the problematic eigenvectors of $A$ are known from *a priori information* (for example because they should vanish), the following iterative procedure may be employed to solve (13.5.1). Starting from an initial estimate $\overline{\mathbf{x}}^{(0)}$, the $j$'th approximation $\mathbf{x}^{(j)}$ is defined as the solution of the system of equations

$$p x_m^{(j)} + \sum_{n=1}^{N} A_{mn}\, x_n^{(j)} = b_m + p \overline{x}_m^{(j-1)} \tag{13.5.4}$$

with $m = 1,2,\ldots,N$. In (13.5.4), $p$ is a real-valued, positive parameter, and $\bar{\mathbf{x}}^{(j-1)}$ is the result of resetting the components of the previous approximation $\mathbf{x}^{(j-1)}$ along the problematic eigenvectors to their a priori known values.

The convergence of this iteration scheme can be analyzed by also expanding the iterates $\{\mathbf{x}^{(j)}\}$ in terms of the eigenvectors $\{\mathbf{v}_\ell\}$. In analogy with (13.5.3), we have

$$\begin{aligned} \mathbf{x}^{(j)} &= \sum_{\ell=1}^{N} \xi_\ell^{(j)} \mathbf{v}_\ell \\ \bar{\mathbf{x}}^{(j)} &= \sum_{\ell=1}^{N} \bar{\xi}_\ell^{(j)} \mathbf{v}_\ell \end{aligned} \tag{13.5.5}$$

Substituting (13.5.5) in (13.5.4) directly yields the recurrence relation

$$\xi_\ell^{(j)} = \frac{\beta_\ell + p\bar{\xi}_\ell^{(j-1)}}{p + \lambda_\ell} \tag{13.5.6}$$

In order to establish whether $\xi_\ell^{(j)}$ is a better approximation to the actual expansion coefficient $\xi_\ell = \lambda_\ell^{-1}\beta_\ell$ than $\bar{\xi}_\ell^{(j-1)}$, we consider how it differs from that solution. From (13.5.6), we have

$$\begin{aligned} \xi_\ell^{(j)} - \lambda_\ell^{-1}\beta_\ell &= \frac{\beta_\ell + p\bar{\xi}_\ell^{(j-1)} - p\lambda_\ell^{-1}\beta_\ell - \beta_\ell}{p + \lambda_\ell} \\ &= \frac{p}{p + \lambda_\ell}\left[\bar{\xi}_\ell^{(j-1)} - \lambda_\ell^{-1}\beta_\ell\right] \end{aligned} \tag{13.5.7}$$

When $\bar{\xi}_\ell^{(j-1)} = \xi_\ell^{(j-1)}$, it follows from (13.5.7) that we have strict convergence if and only if $\lambda_\ell > 0$. Moreover, this convergence property holds regardless of the initial estimate, and for each individual expansion coefficient $\xi_\ell^{(j)}$. The latter observation is especially important since it shows that resetting a particular coefficient $\xi_\ell^{(j)}$ to its a priori known value does not affect the convergence of those remaining.

Finally, (13.5.7) indicates that the components corresponding to the smallest eigenvalues digress the least from their initial estimates. This suggests that, when only a few iteration steps are required to arrive at an acceptable result, it may be possible to leave out the

reset step entirely. In subsequent steps, however, we will then gradually obtain the exact solution (13.5.3), whose inaccuracy initially motivated our taking up the iteration scheme.

The result (13.5.7) rules out the possibility of applying our scheme when one or more of the eigenvalues $\{\lambda_\ell\}$ are negative. In the application that we have in mind, this restriction is not acceptable, since we are not even able to determine all the eigenvalues. However, negative eigenvalues can be handled by redefining $\mathbf{x}^{(j)}$ as the vector that minimizes the squared error

$$\sum_{m=1}^{N} \left\{ \sum_{n=1}^{N} A_{mn}\, x_n^{(j)} - b_m \right\}^2 + p^2 \sum_{m=1}^{N} \left\{ x_m^{(j)} - \overline{x}_m^{(j-1)} \right\}^2 \qquad (13.5.8)$$

Differentiating this error with respect to the individual components $\{x_k^{(j)} \mid k = 1, 2, \ldots, N\}$ reveals that the minimum is obtained when the linear equation

$$p^2 x_k^{(j)} + \sum_{n=1}^{N} \sum_{m=1}^{N} A_{mk}\, A_{mn}\, x_n^{(j)} = \sum_{m=1}^{N} A_{mk}\, b_m + p^2 \overline{x}_k^{(j-1)} \qquad (13.5.9)$$

is satisfied for $k = 1, 2, \ldots, N$. The system of equations (13.5.9) is of the same form as the one given in (13.5.4), the only difference being that the system matrix $A$ is replaced with the result of a left multiplication of $A$ with its transpose. As is well known, such a product matrix has only positive eigenvalues.

It should be noted that each step of the relaxation method is in fact the solution of a regularized version of the linear algebraic equation (13.5.1) [58]. The new element in our solution technique is that, by incorporating this regularized inversion in an iterative scheme, we avoid unnecessary changes in the components of $\mathbf{x}$ along the "well-behaved" eigenvectors. As such, the relaxation method brings about a similar effect as inverting (13.5.1) with the aid of a singular-value decomposition.

### *13.5.2 Application to Transient Scattering Problems*

The properties of the relaxation method found above make this method almost perfectly suited for solving the discretized time-domain integral equation (13.3.3). From the stability analysis of Subsection 13.3.3, we recall that numerically solving this equation can be regarded

as inverting a large, lower-triangular matrix equation, the system matrix of which has a few small eigenvalues with corresponding "problematic" eigenvectors. From (13.3.20), we also have enough information about the behavior of these eigenvectors to "filter out" unwanted components in their direction from the result of each iteration step.

To illustrate the stabilizing effect brought about in the relaxation method, let us reconsider the simplified model introduced in (13.3.16). From (13.5.8), it is observed that a single iteration step of the relaxation method can be modeled by taking, for $n = 0, 1, \ldots, \infty$, the minimum of

$$\left\{ v_j[n] + w_0 C \left( \frac{3}{2} v_j[n] - 2v_j[n-1] + \frac{1}{2} v_j[n-2] \right) \right.$$
$$\left. + w_1 C \left( \frac{3}{2} v_j[n-1] - 2v_j[n-2] + \frac{1}{2} v_j[n-3] \right) - g[n] \right\}^2$$
$$+ p^2 \left( v_j[n] - \overline{v}_{j-1}[n] \right)^2 \qquad (13.5.10)$$

In (13.5.10) $v_j[n]$ represents the approximate time signal found in step $j$ of the relaxation method, and $\overline{v}_{j-1}[n]$ denotes the "corrected" approximation resulting from the previous step.

Differentiating (13.5.10) with respect to $v_j[n]$ results in the modified difference equation

$$(1 + \overline{p}^2) v_j[n] + w_0 C \left\{ \frac{3}{2} v_j[n] - 2v_j[n-1] + \frac{1}{2} v_j[n-2] \right\}$$
$$+ w_1 C \left\{ \frac{3}{2} v_j[n-1] - 2v_j[n-2] + \frac{1}{2} v_j[n-3] \right\} = g[n] + \overline{p}^2 \overline{v}_{j-1}[n] \qquad (13.5.11)$$

where

$$\overline{p}^2 = p^2 / (1 + \frac{3}{2} w_0 C) \qquad (13.5.12)$$

Repeating the stability analysis of Subsection 13.3.3 for the modified difference equation (13.5.11) leads to the conclusion that this equation has a stable solution if and only if

$$0 \leq C \leq (\overline{p}^2 + 1) / (4w_1 - 4w_0) \qquad (13.5.13)$$

This means that, for a given value of the configuration parameter $C$, the regularization parameter $p$ can always be chosen such that solving

(13.5.11) produces a stable result, provided that $g[n]$ and $\overline{v}_{j-1}[n]$ do not have components along the "problematic" eigenvectors.

The only difficulty in applying the relaxation method to the discretized time-domain integral equation (13.3.3) is that the system matrix of (13.3.3) is infinite in the $n$-direction. Therefore, we cannot apply the relaxation method, which involves a multiplication of the system matrix with its transpose, to the full equation. Instead, we utilize the lower-triangular structure of (13.3.3) to apply the relaxation method to subsystems of equations pertaining to field values $\{\tilde{u}(\alpha,n)\}$ at a fixed instant $n$.

This leads to the following procedure for the iterative solution of the system of equations (13.3.3). Starting from a sufficiently smooth estimate $\overline{u}_0(\alpha,n)$, we carry out a number of iteration steps. In step number $j$, the approximate solution $\tilde{u}_j(\alpha,n)$ is obtained as the result of minimizing, for each fixed $n$, the squared error

$$\sum_{\alpha}\left\{\tilde{u}_j(\alpha,n)-\tilde{f}(\alpha,n)-\sum_{\alpha'}\sum_{n'=0}^{n}\tilde{k}(\alpha,\alpha',n-n')\,\tilde{u}_j(\alpha',n')\right\}^2 + p^2\sum_{\alpha}\{\tilde{u}_j(\alpha,n)-\overline{u}_{j-1}(\alpha,n)\}^2 \tag{13.5.14}$$

for known values of $f(\alpha,n)$, $\overline{u}_{j-1}(\alpha,n)$, $\tilde{u}_j(\alpha,n')$ with $n'<n$, and $p$. Differentiating the squared error (13.5.14) with respect to each of the unknown field values $\{\tilde{u}_j(\alpha,n)\}$ results in the system of linear equations

$$\sum_{\alpha'}w_p(\alpha,\alpha')\tilde{u}_j(\alpha',n)=p^2\overline{u}_{j-1}(\alpha,n) + \sum_{\alpha'}w(\alpha',\alpha)\left\{\tilde{f}(\alpha',n)+\sum_{\alpha''}\sum_{n'=0}^{n-1}\tilde{k}(\alpha',\alpha'',n-n')\,\tilde{u}_j(\alpha'',n')\right\} \tag{13.5.15}$$

with

$$w_p(\alpha,\alpha')\overset{\text{def}}{=}p^2\delta_{\alpha\alpha'}+\sum_{\alpha''}w(\alpha'',\alpha)w(\alpha'',\alpha') \tag{13.5.16}$$

In (13.5.15) and (13.5.16), $w(\alpha,\alpha')$ is the weighting matrix defined in (13.3.4).

The system of algebraic equations (13.5.15) is of a similar form as the original marching-on-in-time equations (13.3.3) and (13.3.5), and can be handled numerically in exactly the same way. The only difference between (13.3.5) and (13.5.15) is that solving the latter involves multiplying known terms on the right-hand side with the transpose of the weighting matrix $w(\alpha, \alpha')$ at each instant. Hence, each iteration step in the relaxation method can be envisaged as a modified time-marching computation. Compared with the effort required to carry out the summations approximating the multiple integrals on the right-hand side of (13.3.1), the additional effort involved in the extra matrix multiplications is negligible.

After each iteration step, we must remove the small, unwanted component(s) along the "unstable" eigenvector(s) of the form (13.3.20) from the approximate solution obtained. This is achieved by carrying out a smoothing operation that consists of replacing $\tilde{u}_j(\alpha, n)$ with

$$\overline{u}_j(\alpha, n) \stackrel{\text{def}}{=} [\tilde{u}_j(\alpha, n-1) + 2\tilde{u}_j(\alpha, n) + \tilde{u}_j(\alpha, n+1)]/4 \qquad (13.5.17)$$

for $0 < n < \infty$. This smoothing operation is based on linear interpolation in time, and, hence, is accurate up to $\mathcal{O}(h^2)$. This makes the error induced by the correction consistent with the discretization error specified at the beginning of Subsection 13.3.5. If necessary, the smoothing operation can be repeated several times.

This iterative procedure should not be confused with solving, for a fixed $n$, (13.5.15) repeatedly until convergence for known (converged) values of $\tilde{u}_j(\alpha, n')$ with $n' < n$. The latter procedure is equivalent to solving (13.3.3), and, hence, will produce the unstable time-marching result that we aimed at avoiding. The improvement in our iterative procedure is that, by computing in each iteration step $\tilde{u}_j(\alpha, n)$ for *all* $n$, we are able to apply the smoothing procedure that removes the component(s) along the problematic eigenvector(s) of the system of equations (13.3.3).

A consequence of this strategy is that the iterative procedure will start to converge at the beginning of the time interval under consideration, and will gradually produce results that are accurate over a longer subinterval. For very fine space-time meshes in particular, this may have the effect that, in the initial iteration steps, spurious wavelets are built up at late times. The elimination of such wavelets in subsequent iterations may even cause the global root-mean-square error (13.4.5) to grow temporarily with increasing $j$, in spite of the fact that the

approximate result $\tilde{u}_j(\alpha, n)$ is actually improving. An example will be given in Subsection 13.5.3.

The only remaining question is the choice of a suitable value for the relaxation parameter $p$. This value must be determined by trial and error in the first iteration step. When the instabilities do not show up in that step, we may expect them not to turn up in subsequent steps either.

The essential difference between the relaxation method and the conjugate-gradient method is that the relaxation method produces, in each iteration step, a *partial* improvement along *all* well-behaved eigenvectors. A gradient-type method, on the other hand, produces a *total* improvement in a *single* direction. The common element in both methods is that they will produce similar *global* errors.

The principal difference between the relaxation method and Rao's approach is that the former suppresses the unwanted components from the successive iterates on the basis of the *temporal* behavior, and the latter on the basis of the *spatial* behavior. As remarked in Subsection 13.4.5, considering the spatial behavior may not provide a sufficient separation. The temporal behavior, on the other hand, is completely known from the stability analysis of Subsection 13.3.3, and is essentially different for the stable and the unstable parts of $\tilde{u}_j(\alpha, n)$.

### *13.5.3 Examples*

As in the previous two sections, our theoretical observations have been confirmed numerically. To this end, we have applied the relaxation method to the "tutorial" problem of scattering by a slab, and to the corresponding two-dimensional problem of scattering by an inhomogeneous, lossy dielectric cylinder in free space. This means solving discretized versions of the integral equations (13.2.64) and (13.2.67).

In all computations, the iterative procedure was started from the initial value $\bar{u}_0(\alpha, n) = 0$. Since this initial value has zero components along all eigenvectors of the system matrix of (13.3.3), it certainly fulfills the requirement that it should have zero components along the problematic ones. Moreover, making the same choice as in (13.4.6) and (13.4.11) facilitates the comparison of the various methods discussed in this chapter.

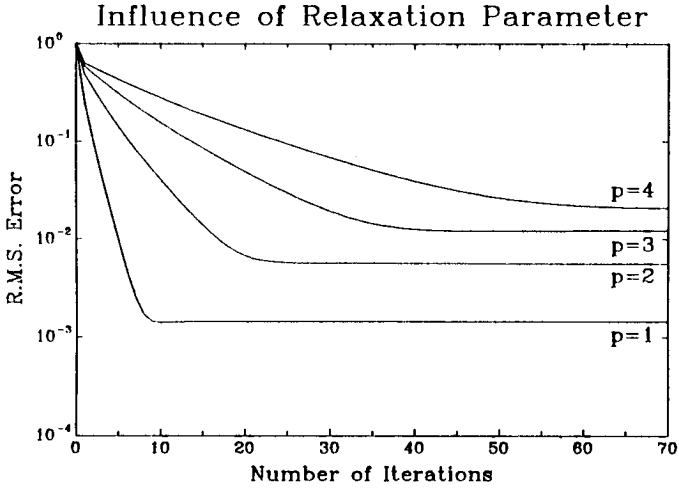


**Figure 13.5.1 Dependence of the rate of convergence on the relaxation parameter $p$. The configuration is a homogeneous, lossless dielectric slab with $\epsilon_{2r} = 2.25$ in free space, excited by a sine-squared incident pulse of duration $c_0 T/d = 2$, and subdivided into $M = 40$ subintervals.**

## *Dielectric Slab*

Starting with the case of the slab, we first investigate the influence of the relaxation parameter $p$. For the same configuration that was considered in Fig. 13.4.2, we have, for $M = 40$, applied the relaxation method with $p = 1, 2, 3, 4$. After each iteration step, we performed the smoothing operation given in (13.5.17) a single time. The convergence of the successive iterates is demonstrated in Fig. 13.5.1. For consistency, we use the same root-mean-square error as in Section 13.4, i.e. the one defined in (13.4.5).

Figure 13.5.1 demonstrates two characteristic features of the relaxation method. In the first place, the rate of convergence decreases with increasing $p$. This can be understood from the fact that the second term in the squared error (13.5.14) becomes increasingly more important as $p$ increases. In the second place, the root-mean-square error approaches a fixed level as the iterative procedure progresses. The interpretation of this phenomenon is that, upon convergence of the relaxation method, a balance sets in between the correction achieved in each iteration step and the distortion brought about by the smoothing operation. The larger final value of the root-mean-square error for

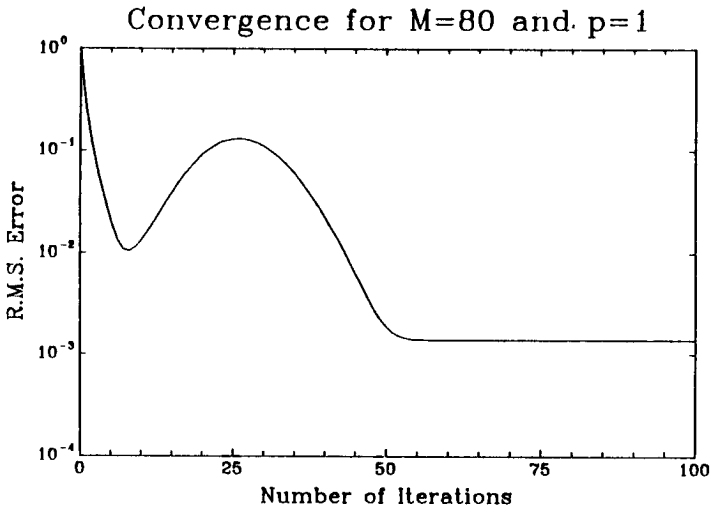


**Figure 13.5.2 Convergence of the relaxation method for a fine space-time mesh. The configuration is a homogeneous, lossless dielectric slab with $\epsilon_{2r} = 2.25$ embedded in free space, excited by a sine-squared incident pulse of duration $c_0T/d = 1$. The computations were carried out for $p = 1$ and $M = 80$.**

larger values of $p$ corresponds to the deceleration of the convergence.

As in Subsection 13.4.4, we studied the influence of the discretization, the duration of the incident pulse, and the permittivity of the slab. Refining the discretization has no significant effect of the initial rate of convergence. For very fine meshes, however, the root-mean-square error may temporarily grow before it decays to its final value. An example is shown in Fig. 13.5.2.

The growth in the root-mean-square error is caused by the occurrence of spurious wavelets at late times mentioned in Subsection 13.5.2. In Figure 13.5.3, we have plotted, as an illustration, the reflected and transmitted fields obtained after 25 iterations, when the root-mean-square error is near its maximum, and after 100 iterations. In connection with these results, it should be remarked that, although each iteration of the relaxation method changes the solution $\tilde{u}_j(\alpha, n)$ over the entire time interval of interest, the actual improvement is confined to a subinterval. Consequently, a global error of the type (13.4.5) may not be an appropriate yardstick for measuring the improvement in $\tilde{u}_j(\alpha, n)$.

Turning our attention to the physical parameters, it turns out

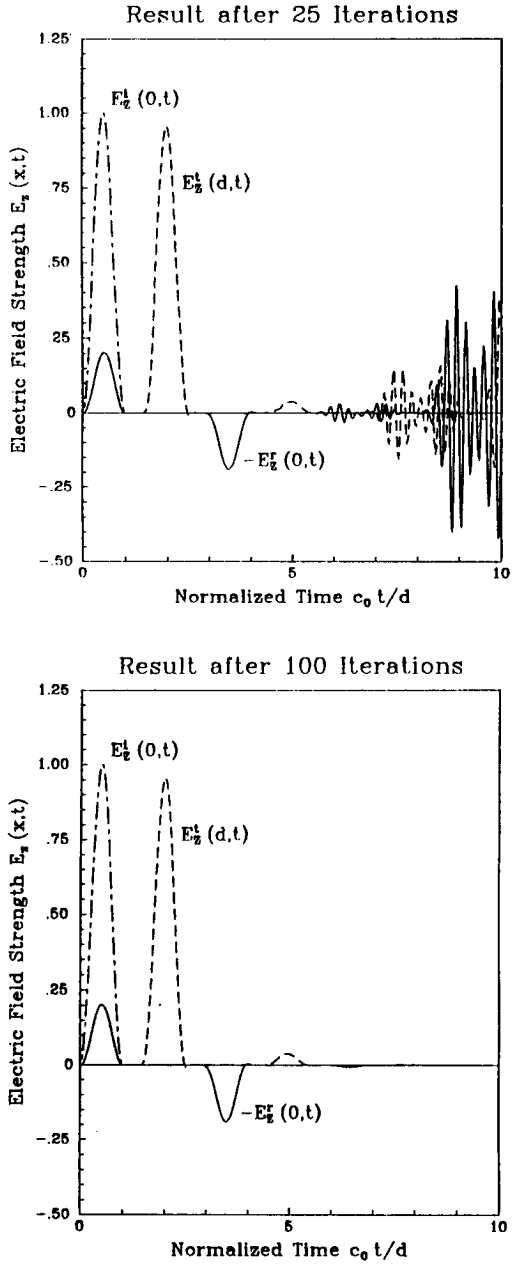


**Figure 13.5.3 Occurrence and disappearance of spurious wavelets at late times as observed in applying the relaxation method for a fine space-time discretization. The configuration is a homogeneous, lossless slab with $\epsilon_{2r} = 2.25$ in free space, excited by a sine-squared incident pulse of duration $c_0 T/d = 1$. The computations were carried out for $p = 1$ and $M = 80$.**

that the convergence of the relaxation method is hardly affected by the duration of the incident pulse. Enlarging the susceptibility of the slab even results in a faster convergence, in spite of the fact that the desired time-domain field extends over a longer time interval. This is just as well, since the stability condition (13.5.13) prescribes that, when the results are actually unstable, raising the value of the susceptibility must go together with augmenting the relaxation parameter $p$.

*Dielectric Cylinder*

To prove that the relaxation method is really capable of stabilizing time-domain computations, we have also applied it to the one problem discussed in Subsections 13.2.3, 13.2.4 and 13.3.5 for which the marching-on-in-time method is inherenty unstable, i.e. the dielectric cylinder specified in connection with (13.2.64).

Figure 13.5.4 shows results for the same situation as specified in Fig. 13.3.4. Now, the dimensionless conductivity has been increased to $Z_0\sigma a = 10$, which exceeds the upper limit of the stability range for the marching-on-in-time method for the pertinent discretization by a factor of 2. From the upper half of Fig. 13.5.4, it is observed that, after ten iteration steps, the iterative result meets the equality sign in the discretized integral equation with a global accuracy of three significant digits. Note that performing the 15 iteration steps takes about half the computational effort required in applying the marching-on-in-time method with a twice-refined discretization, which is the least we would have to do to extend the stability range of that technique by a factor of two.

The results shown in Fig. 13.5.4 may also serve to demonstrate the poor condition of the discretized integral equation. As remarked above, the smooth solution of Fig. 13.5.4 meets the equality sign of that equation with an average accuracy of about $10^{-3}$. On the other hand, the exact solution to the discretized equation is dominated by a large, alternating unstable component. This is in complete agreement with the matrix interpretation of Subsection 13.3.3, that this unstable component can be associated with an eigenvector of the system matrix of the discretized equation with a small eigenvalue.

In Figure 13.5.5, we consider the same discretized equation as in the lower half of Fig. 13.3.5 with a three times larger susceptibility, i.e. $\chi = 5$. The most interesting aspect of this particular application is that, according to Fig. 13.3.5, we must now suppress an interplay of

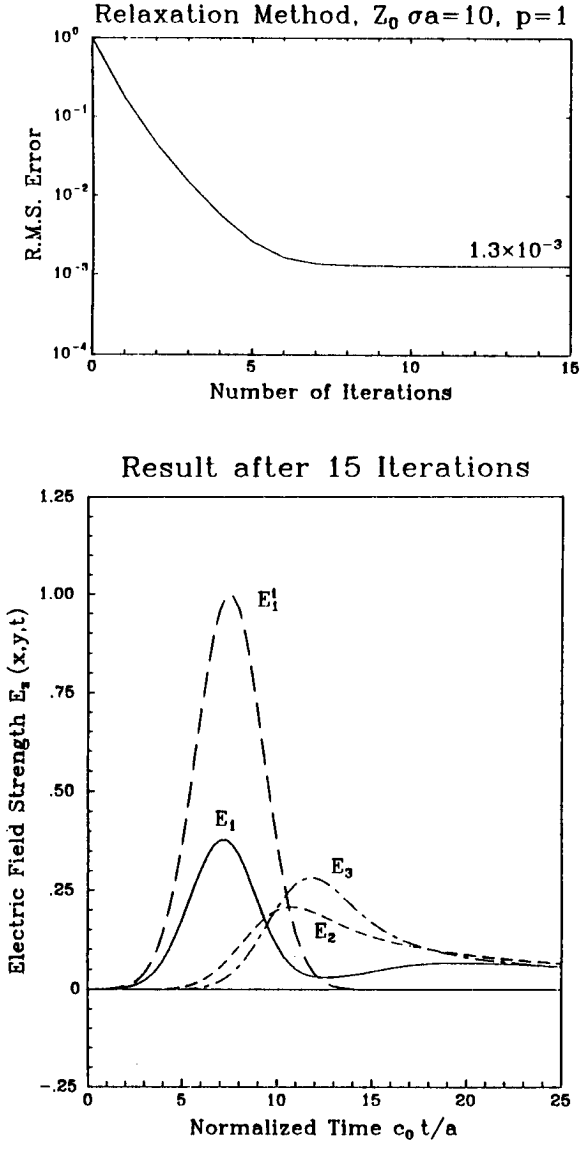


**Figure 13.5.4 Results of applying the relaxation method to obtain the field excited by a Gaussian pulse of duration $c_0T/a = 10$ in a homogeneous, square cylinder of width $2a$ with $\chi = 0$ and $Z_0\sigma a = 10$. The computations were carried out for $p = 1$ and $M = 3$. Point 1 $= (-a, 0)$, Point 2 $= (0, 0)$, Point 3 $= (a, 0)$.**

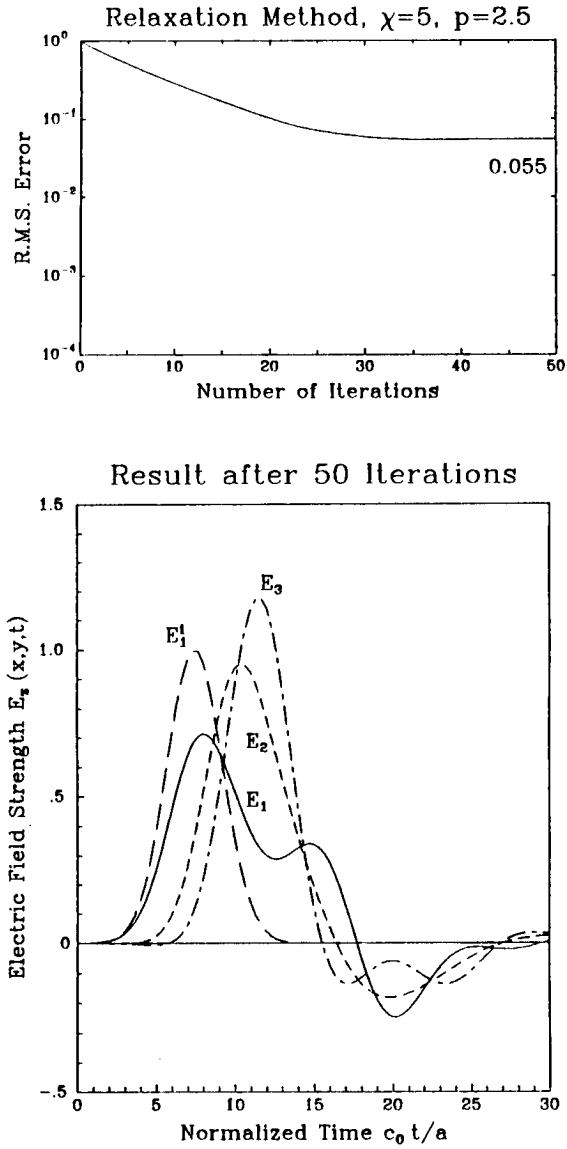


**Figure 13.5.5 Results of applying the relaxation method with $p = 2.5$ to obtain the field excited by a Gaussian pulse of duration $c_0T/a = 10$ in a homogeneous, square cylinder of width $2a$, with $\chi = 5$, $\sigma = 0$, $M = 3$, and the time differentiations discretized with the double time step. Point 1 = $(-a, 0)$, Point 2 = $(0, 0)$, Point 3 = $(a, 0)$.**

instabilities alternating with the double time step. This is achieved by carrying out the smoothing operation (13.5.17) two times after each iteration of the relaxation method. As Figure 13.5.5 indicates, a stable result can be obtained for $p = 2.5$. The larger residual value of the root-mean-square error is due to the more rapid variation of the exact field $\mathcal{E}_z$ with $\rho$ and $t$, which results in a larger discretization error.

In connection with Fig. 13.5.5, finally, it should be remarked that the smoothing operation (13.5.17) is an effective, but relatively crude low-pass filtering procedure. It seems possible, therefore, to come up with a less radical procedure for removing the unwanted alternating behavior given by (13.3.20) from the successive iterates. Perhaps, using such a procedure would avoid some of the over-smoothing effects that show up in Fig. 13.5.5.

## 13.6 Conclusions

In this chapter, we have presented a systematic formulation of integral equations for the description of electromagnetic transient-scattering problems as well as techniques for the numerical solution of such equations. The derivation of the integral equations is carried out with the aid of a spatial Fourier transformation of the space-time electromagnetic-field equations over a finite domain, and a temporal Laplace transformation over a semi-infite interval.

The numerical schemes comprise the marching-on-in-time method, which is a direct procedure based on the principle of causality, as well as the conjugate-gradient method and the relaxation method, both of which solve the problem iteratively. A matrix interpretation has been proposed that provides a detailed understanding of the theoretical as well as the practical aspects of each of these methods. In addition, all of our theoretical observations have been confirmed numerically.

At the first glance, it seems most attractive to solve transient-scattering problems directly, by marching on in time. However, the accumulation of discretization errors as the time-domain updating procedure progresses may give rise to exponentially increasing instabilities. For some configurations, either the discretization of the integral equation or the problem formulation can be modified such that these instabilities are avoided. On the other hand, configurations exist for which

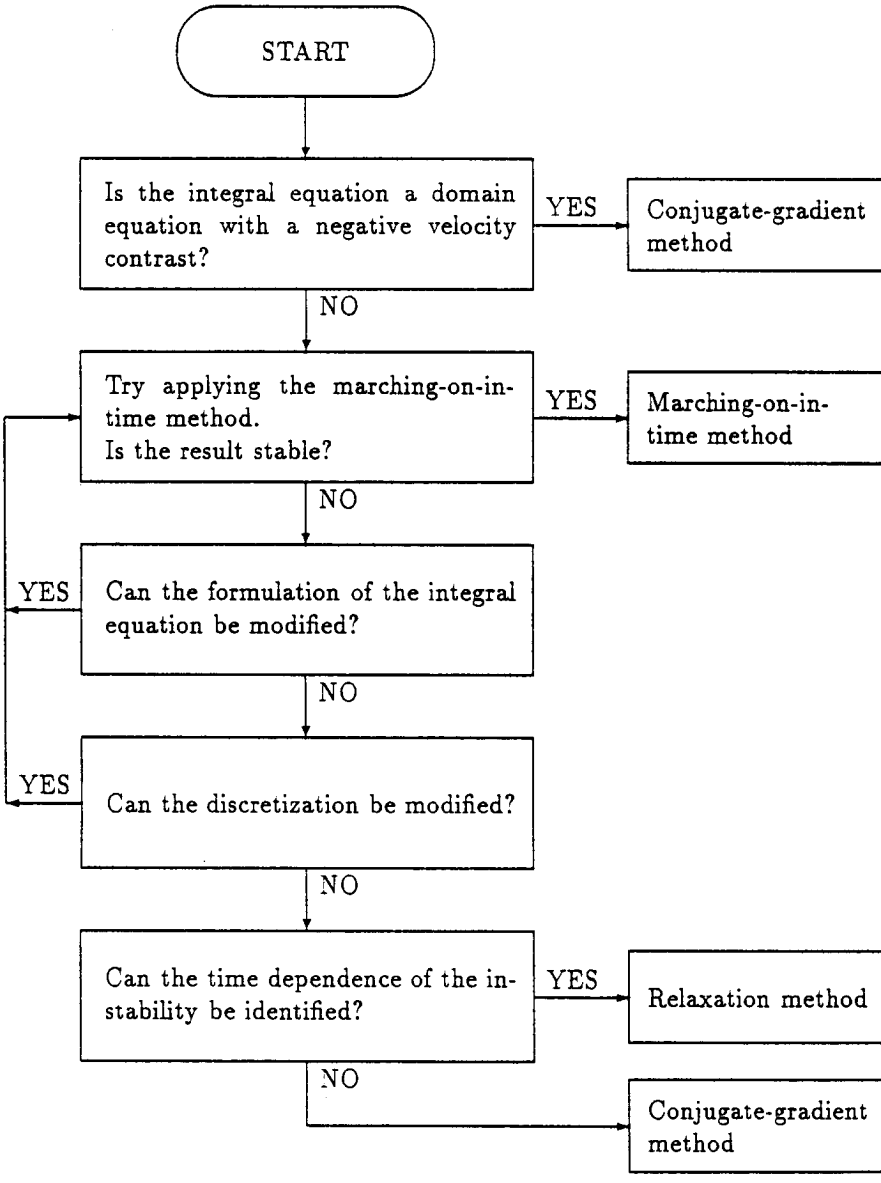


**Figure 13.6.1 Decision tree for selecting the most appropriate numerical procedure for solving a given time-domain integral equation.**

neither modification leads to a stable result. Of the examples discussed in this chapter, the dielectric slab and the two- and three-dimensional impenetrable obstacles appear to fall into the former category, and the dielectric cylinder into the latter.

Both iterative procedures have the advantage that the instabilities encountered in the marching-on-in-time method are inherently avoided, albeit at the cost of a considerable increase in computational effort. The conjugate-gradient method does not suffer from instabilities because of its global character, which restricts the successive iterates to field distributions that are negligible outside a finite time interval. However, because of the vast dimension of the space of possible solutions, it may take a large number of iterations to arrive at an acceptable solution. Moreover, each iteration step requires an effort equivalent to performing two complete marching-on-in-time computations over a time interval that is twice long as the one of actual interest. A specific advantage of the conjugate-gradient method is that, because of its global character, only this method is capable of solving domain integral equations with a negative velocity contrast. This makes it the only time-domain integral-equation method available for solving transient scattering by e.g. voids in dielectric media.

The relaxation method was taylored directly to time-domain scattering problems, and amounts to a regularized solution of the discretized integral equation in matrix form. The method seems generally applicable, provided that the approximate behavior of the unstable part of the solutions is known. Compared with the conjugate-gradient method, it seems more suitable for the determination of a large solution vector, since it operates on all components of that vector simultaneously, as opposed to achieving total improvement in a single direction. Moreover, each iteration step requires only an effort equivalent to carrying out a single marching-on-in-time computation over the time interval of interest.

A somewhat surprising result of our analysis is that, with respect to the global error in the solutions obtained, the three methods are almost equivalent. In fact, when the marching-on-in-time method produces a stable result, applying either iterative method with the same space-time discretization will eventually lead to precisely that result. In view of the difference in numerical efficiency therefore, it seems almost mandatory to first investigate all possibilities of constructing a stable time-marching scheme. Only when this investigation is unsuc-

cessful should an iterative solution be considered. The effort spent in the numerical implementation will not be lost, since the computation of the source-type integrals, which takes up most of the work, can form the basis of the implementation of both iterative procedures as well.

These conclusions have been summarized in the decision tree of Fig. 13.6.1. Given a particular time-domain integral equation, this decision tree offers the reader a suggestion as to which numerical method has the best chance of success. It is admittedly somewhat speculative, but it is the best assessment that can be given at the present time.

## Acknowledgments

The author would like to thank Professor Tapan K. Sarkar for his suggestion to write this chapter. Further, he would like to thank his colleagues of the Laboratory of Electromagnetic Research, Department of Electrical Engineering, Delft University of Technology, for many stimulating discussions. In particular, he is indebted to Professor Hans Blok, for his permanent interest during the progress of this work, and to Professor Peter M. Van den Berg, for his clear explanation of conjugate-gradient methods. Finally, the careful remarks of Dr. Dominique Lesselier from the Ecole Supérieure d'Electricité, Gif-sur-Yvette, France, and of Dr. Amelia Rubio Bretones from the Universidad de Granada, Granada, Spain, are gratefully acknowledged.

## References

[1] Friedman, M. B., and R. P. Shaw, "Diffraction of pulses by cylindrical obstacles of arbitrary cross section," *J. Appl. Mech.*, **29**, 40–46, 1962.

[2] Shaw, R. P., "Diffraction of acoustic pulses by obstacles of arbitrary shape with a Robin boundary condition," *J. Acoust. Soc. Am.*, **41**, 855–859, 1967.

[3] Shaw, R. P., "Diffraction of plane acoustic pulses by obstacles of arbitrary cross section with an impedance boundary condition," *J. Acoust. Soc. Am.*, **44**, 1062–1068, 1968.

[4] Shaw, R. P., "Transient scattering by a circular cylinder," *J. Sound Vibr.*, **42**, 295–304, 1975.

[5] Mitzner, K. M., "Numerical solution for transient scattering from a hard surface of arbitrary shape - Retarded potential technique," *J. Acoust. Soc. Am*, **42**, 391–397, 1967.

[6] Neilson, H. C., Y. P. Lu and Y. F. Wang, "Transient scattering by axisymmetric surfaces," *J. Acoust. Soc. Am.*, **63**, 1719–1726, 1978.

[7] Bennett, C. L., and H. Mieras, "Time domain integral equation solution for acoustic scattering from fluid targets," *J. Acoust. Soc. Am.*, **69**, 1261–1265, 1981.

[8] Bennett, C. L., and H. Mieras, "Space-time integral equation solution for hard or soft targets in the presence of a hard or soft half space," *Wave Motion*, **5**, 399–411, 1983.

[9] Bennett, C. L., *A technique for computing approximate impulse response of conducting bodies*, Ph.D. Thesis, Purdue University, Lafayette, Indiana, 1968.

[10] Bennett, C. L., and W. L. Weeks, "Transient scattering from conducting cylinders," *IEEE Trans. Antennas Propagat.*, **AP-18**, 627–633, 1970.

[11] Bennett, C. L., and H. Mieras, "Time domain scattering from open thin conducting surfaces," *Radio Sci.*, **16**, 1231–1239, 1981.

[12] Tijhuis, A. G, "Toward a stable marching-on-in-time method for two-dimensional transient electromagnetic scattering problems," *Radio Sci.*, **19**, 1311–1317, 1984.

[13] Damaskos, N. J., R. T. Brown, J. R. Jameson, and P. L. E. Uslenghi, "Transient scattering by resistive cylinders," *IEEE Trans. Antennas Propagat.*, **AP-33**, 21–25, 1985.

[14] Poggio, A. J., and E. K. Miller, "Integral equation solutions of three-dimensional scattring problems." In: *Computer techniques for electromagnetics*, R. Mittra (ed.), Pergamon Press, Oxford, Chap. 4, 1973.

[15] Mittra, R., "Integral equation methods for transient scattering." In: *Transient electromagnetic fields*, L.B. Felsen (ed.), Springer Verlag, Berlin, Chap. 2, 1976.

[16] Bennett, C. L., "The numerical solution of transient electromagnetic scattering problems." In: *Electromagnetic Scattering*, P.L.E. Uslenghi (ed.), Academic Press, New York, Chap. 11, 1978.

[17] Bennett, C. L., and G. F. Ross, "Time-domain electromagnetics and its applications," *Proc. IEEE*, **66**, 299–318, 1978.

[18] Mieras, H., and C. L. Bennett, "Space-time integral approach to dielectric targets," *IEEE Trans. Antennas Propagat.*, **AP-30**, 2–9, 1982.

[19] Marx, E., "Integral equation for scattering by a dielectric," *IEEE Trans. Antennas Propagat.*, **AP-32**, 166–172, 1984.

[20] Herman, G. C., "Scattering of transient acoustic waves by an inhomogeneous obstacle," *J. Acoust. Soc. Am*, **69**, 909–915, 1981.

[21] Herman,G. C., *Scattering of transient acoustic waves in fluids and solids*, Ph.D. Thesis, Delft University of Technology, Delft, The Netherlands, 1981.

[22] Herman, G. C., "Scattering of transient elastic waves by an inhomogeneous obstacle: Contrast in volume density and mass," *J. Acoust. Soc. Am*, **71**, 264–272, 1982.

[23] Lesselier, D., "*P* waves transient scattering by 2-D penetrable targets: A direct solution," *J. Acoust Soc. Am*, **74**, 1274–1278, 1983.

[24] Bolomey, J. Ch., Ch. Durix, and D. Lesselier, "Time domain integral equation approach for inhomogeneous and dispersive slab problems," *IEEE Trans. Antennas Propagat.*, **AP-26**, 658–667.

[25] Lesselier, D., *Diagnostic optimal de la lame inhomogène en régime temporel. Applications à l'électromagnétisme et à l'acoustique*, Ph.D. Thesis, l'Université Pierre et Marie Curie, Paris, 1982.

[26] Tijhuis, A. G, "Iterative determination of permittivity and conductivity profiles of a dielectric slab in the time domain," *IEEE Trans. Antennas Propagat.*, **AP-29**, 239–245, 1981.

[27] Dohner, J. L., R. Shoureshi, and R. J. Bernard, "Transient analysis of three-dimensional wave propagation using the boundary element method," *International Journal for Numerical Methods in Engineering*, **24**, 621–634, 1987.

[28] Marx, E., "Self-patch integrals in transient electromagnetic scattering," *IEEE Trans. Antennas Propagat.*, **AP-33**, 763–767, 1985.

[29] Marx, E., "Neighboring-patch integrals in transient electromagnetic scattering," *IEEE Trans. Antennas Propagat.*, **AP-33**, 768–773, 1985.

[30] Rynne, B. P., "Stability and convergence of time marching methods in scattering problems," *IMA J. Appl. Math.*, **35**, 297–310, 1985.

[31] Herman, G. G., and P. M. van den Berg, "A least-square iterative technique for solving time-domain scattering problems," *J. Acoust. Soc. Am.*, **72**, 1947–1953, 1982.

[32] van den Berg, P. M., "Iterative computational techniques in scattering based upon the integrated square error criterion," *IEEE Trans. Antennas Propagat.*, **AP-32**, 1063–1071, 1984.

[33] van den Berg, P. M., "Iterative schemes based on the minimization of the error in field problems," *Electromagnetics*, **5**, 237–262, 1985.

[34] Sarkar, T. K., "The application of the conjugate gradient method to the solution of operator equations arising in the electromagnetic scattering from wire antennas," *Radio Sci.*, **19**, 1156–1172, 1984.

[35] Sarkar, T. K., and S. M. Rao, "The application of the conjugate gradient method for the solution of elelctromagnetic scattering from arbitrarily oriented wire antennas," *IEEE Trans. Antennas Propagat.*, **AP-32**, 398–403, 1984.

[36] Rao, S. M., T. K. Sarkar, and S. A. Dianat, "The application of the conjugate gradient method to the solution of transient electromagnetic scattering from thin wires," *Radio Sci.*, **19**, 1319–1326, 1984.

[37] Tijhuis, A. G., *Electromagnetic Inverse Profiling: Theory and Numerical Implementation*, VNU Science Press, Utrecht, The Netherlands, 1987.

[38] De Hoop, A. T., "General considerations on the integral-equation formulation of diffraction problems." In: *Modern topics in electromagnetics and antennas*, E.J. Maanders and R. Mittra (eds.), PPL Conference Publications 13, Peter Peregrinus, Stevenage, U.K., Chap. 6, 1977.

[39] Widder, D. V., *The Laplace Transform*, Princeton University Press, Princeton, 61–63, 1946.

[40] De Hoop, A. T., "A modification of Cagniard's method for solving seismic pulse problems," *Appl. Sci. Res.*, **3**, 179–188, 1960.

[41] Achenbach, J. D., *Wave propagation in elastic solids*, North-Holland Publishing Company, Amsterdam, 298, 1973.

[42] Van der Hijden, J. H. M. T, *Propagation of transient elastic waves in stratified anisotropic media*, North-Holland Publishing Company, Amsterdam, 1987.

[43] De Hoop, A. T., "Acoustic radiation from impulsive point sources in a layered fluid," *Nieuw Archief voor Wiskunde*, **6**, 111–129, 1988.

[44] Rynne, B. P., "Instabilities in time marching methods for scattering problems," *Electromagnetics*, **6**, 129–144, 1986.

[45] Marx, E., "Electromagnetic pulse scattered by a sphere," *IEEE Trans. Antennas Propagat.*, **AP-35**, 412–417, 1987.

[46] Hildebrand, F. B., *Introduction to numerical analysis*, McGraw-Hill, New York, Chap. 3, 1956.

[47] Press, W. H., B. P. Flannery, S. A. Teukolsky, and W. T. Vetterling, *Numerical Recipes*, Cambridge University Press, Cambridge, Chap. 17, 1986.

[48] Abramowitz, M. A., and I. A. Stegun, *Handbook of mathematical functions*, Dover Publications, New York, 1965.

[49] Tijhuis, A. G, R. Wiemans, and E. F. Kuester, "A hybrid method for solving time-domain integral equations in transient scattering," *Journal of Electromagnetic Waves and Applications*, **9**, 495–511, 1989.

[50] Heyman, E., and Felsen, L. B., "Creeping waves and resonances in transient scattering by smooth convex objects," *IEEE Trans. Antennas Propagat.*, **AP-31**, 426–437, 1983.

[51] Yaghjian, A. D., "Augmented electric- and magnetic-field integral equations," *Radio Sci.*, **16**, 987–1001, 1981.

[52] Smith, P. D., "Stable numerical methods for integral equations governing the scattering of transients," *Bulletin IMA 24*, 166–170, 1988.

[53] Smith, P. D., "Instabilities in time-marching methods for scattering - Cause and rectification," submitted for publication in *Elec-*

[40] De Hoop, A. T., "A modification of Cagniard's method for solving seismic pulse problems," *Appl. Sci. Res.*, **3**, 179–188, 1960.

[41] Achenbach, J. D., *Wave propagation in elastic solids*, North-Holland Publishing Company, Amsterdam, 298, 1973.

[42] Van der Hijden, J. H. M. T, *Propagation of transient elastic waves in stratified anisotropic media*, North-Holland Publishing Company, Amsterdam, 1987.

[43] De Hoop, A. T., "Acoustic radiation from impulsive point sources in a layered fluid," *Nieuw Archief voor Wiskunde*, **6**, 111–129, 1988.

[44] Rynne, B. P., "Instabilities in time marching methods for scattering problems," *Electromagnetics*, **6**, 129–144, 1986.

[45] Marx, E., "Electromagnetic pulse scattered by a sphere," *IEEE Trans. Antennas Propagat.*, **AP-35**, 412–417, 1987.

[46] Hildebrand, F. B., *Introduction to numerical analysis*, McGraw-Hill, New York, Chap. 3, 1956.

[47] Press, W. H., B. P. Flannery, S. A. Teukolsky, and W. T. Vetterling, *Numerical Recipes*, Cambridge University Press, Cambridge, Chap. 17, 1986.

[48] Abramowitz, M. A., and I. A. Stegun, *Handbook of mathematical functions*, Dover Publications, New York, 1965.

[49] Tijhuis, A. G, R. Wiemans, and E. F. Kuester, "A hybrid method for solving time-domain integral equations in transient scattering," *Journal of Electromagnetic Waves and Applications*, **9**, 495–511, 1989.

[50] Heyman, E., and Felsen, L. B., "Creeping waves and resonances in transient scattering by smooth convex objects," *IEEE Trans. Antennas Propagat.*, **AP-31**, 426–437, 1983.

[51] Yaghjian, A. D., "Augmented electric- and magnetic-field integral equations," *Radio Sci.*, **16**, 987–1001, 1981.

[52] Smith, P. D., "Stable numerical methods for integral equations governing the scattering of transients," *Bulletin IMA 24*, 166–170, 1988.

[53] Smith, P. D., "Instabilities in time-marching methods for scattering - Cause and rectification," submitted for publication in *Elec-*

*tromagnetics.*

[54] Dudley, D. G., "Error minimization and convergence in numerical methods," *Electromagnetics*, 5, 89–97, 1985.

[55] van den Berg, P. M., "Iterative schemes based on minimization of a uniform error criterion," This Volume, Chap. 2.

[56] Gill, P. E., W. Murray, and M. H. Wright, *Practical Optimization*, Academic Press, London, Chap. 4, 1981.

[57] Rao, S. K., T. K. Sarkar, and S. A. Dianat, "A novel technique to the solution of transient electromagnetic scattering from thin wires," *IEEE Trans. Antennas Propagat.*, **AP-34**, 630–634, 1986.

[58] Tikhonov, A. N., and V. Y. Arsenin, *Solutions of ill-posed problems*, V.H. Winston & Sons, Washington D.C., 1977, Chapters II, III.